Uranium and europium sorption on amidoxime-functionalized magnetic chitosan micro-particles

Mohammed F Hamza, Jean-Claude Roux, Eric Guibal

Uranium and europium sorption on amidoxime-functionalized magnetic chitosan micro-particles

Mohammed F. Hamza[a,b], Jean-Claude Roux[a], Eric Guibal[a,*]

[a] C2MA, IMT Mines Ales, Univ. Montpellier, Alès, France
[b] Nuclear Materials Authority, POB 530, El-Maadi, Cairo, Egypt

HIGHLIGHTS

- Magnetic chitosan functionalized by grafting amidoxime groups for metal sorption.
- Selectivity for U/Eu separation controlled by pH.
- Stable sorption/desorption properties over 5 cycles.
- Langmuir and pseudo-second order rate equations for modeling isotherm and kinetics.
- Successful uranium recovery from alkaline leachate of dolostone ore.

GRAPHICAL ABSTRACT

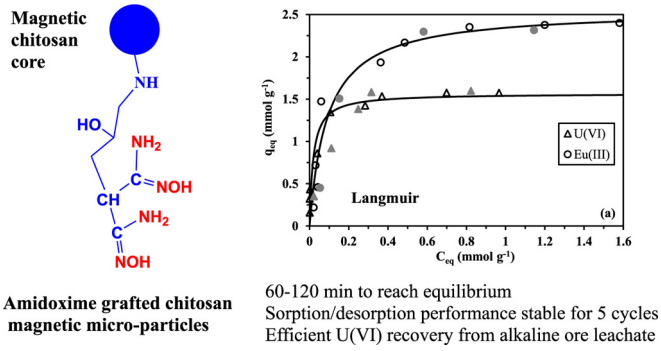

ABSTRACT

Keywords:
Uranyl(VI) ions
Eu(III) ions
Amidoximated-chitosan
Sorption isotherms
Uptake kinetics
Desorption efficiency
Sorbent recycling

Magnetic chitosan particles were successfully modified by amidoxime-grafting (as evidenced by FTIR analysis, SEM-EDX analysis, elemental analysis, X-ray diffraction (XRD), thermogravimetric analysis and titration). The effect of pH was investigated showing optimum sorption at pH 4 for U(VI) and pH 5 for Eu(III). Uptake kinetics are relatively fast: the equilibrium was reached within 60–90 min; and the kinetic profiles were preferentially fitted by the pseudo-second order rate equation. Sorption isotherms are equally fitted by the Langmuir and the Sips equations; under optimal conditions maximum sorption capacity reaches 1.5 mmol U g^{-1} and 2.47 mmol Eu g^{-1}. In bi-component solution, at pH close to 4.9, uranyl is enriched on the sorbent (higher selectivity coefficient) while maintaining high sorption capacities. The selectivity for Eu(III) sorption is higher at pH 2.3 but at the expense of a decrease in sorption capacities. Metal ions can be readily and fast desorbed using 0.5 M HCl solutions: 30–90 min are sufficient for achieving the complete desorption of U(VI) and about 95% of Eu(III) desorption. Sorption and desorption performances are maintained almost constant over 5 cycles of sorption/desorption: the sorbent can be efficiently recycled. Uranium was successfully recovered from alkaline leachate of a sedimentary dolostone ore material.

1. Introduction

The increasing demand for rare-earths metals due to their wide utilization in high-tech industries, the strategic criterion associated to uranium resource are making necessary the development of alternative methods for their recovery from primary resources and for their recycling from waste materials. Mining and metallurgical activities are facing problems for the competitive recovery of strategic metals in the

processing of low-grade resources [1]. Low-grade ores, reprocessed ores and spent materials are usually characterized by the presence of low levels of strategic metals, or hazardous materials; their recovery by leaching or bioleaching produces low-metal concentration leachates that cannot be valorized by conventional processes. Indeed, solvent extraction is usually poorly competitive for diluted effluents and environmentally hazardous due to the loss of extractants by partial solubility in water [2–4]. Precipitation is rarely selective, especially in the case of complex multi-component solutions that contain high levels of base metals and poor content of strategic metals. For these reasons, sorption processes are frequently preferred for the treatment of dilute solutions using ion-exchange and chelating resins [5–10], extractant impregnated materials [11–13], mineral sorbents [14–18], carbon-based sorbents [19–21] or biosorbents [22–27].

In the field of uranium recovery amidoxime-based resins have retained a great attention because of their high affinity for this metal [9,28–31], including in very complex solutions such as seawater [32,33]. Despite the low concentration of uranium and high salinity in marine waters, amidoxime-based resins are able to strongly concentrate the metal [32–37]. Amidoxime resins have retained much less attention for the recovery of heavy metals [38–44], and even less for the binding of rare earth elements [45–49].

Chitosan is an aminopolysaccharide characterized by the presence of numerous hydroxyl and amine groups that confer to the biopolymer an interesting hydrophilic behavior and strong reactivity for metal binding through different mechanisms. In addition, these reactive groups offer possibilities for chemical modification and grafting of specific reactive groups. Free electron doublet on nitrogen of amine groups bind metal cations by chelation in near neutral solutions while the protonation of amine groups in acidic solutions improves the sorption of metal anions by ion-exchange/electrostatic attraction mechanisms [50]. The protonation of amine groups in acidic solutions involves biopolymer dissolving in aqueous solutions (with the remarkable exception of sulfuric acid), which, in turn, facilitates the shaping and conditioning of the polymer for the preparation of membranes, beads, fibers, hollow fibers [50] and foams [51]. This contributes also to develop encapsulation process for the immobilization of ion-exchangers [52], the coating of solid supports [53] or the functionalization of magnetic core particles [54]. The main drawback of chitosan in terms of sorption processing consist of the poor porosity of raw biopolymer; this means significant limitation is mass transfer properties that can be run out by conditioning the biopolymer as hydrogels and by appropriate drying. Freeze-drying and drying under supercritical CO_2 conditions allow maintaining, at least partially, the original porosity [55]. An alternative way to limit the resistance to intraparticle diffusion consists of reducing the size of the sorbent particles. In this case, the resulting sorbent cannot be used in fixed-bed columns; due to head loss pressure and hydrodynamic blockage, while in batch systems the solid/liquid separation is made complex when processing very small particles. Preparing magnetic particles allows both easy solid/liquid separation and optimized diffusion properties [56–59].

This study focuses on the synthesis of magnetic chitosan microparticles that are further functionalized by grafting malonitrile (through the intermediary grafting of epichlorohydrin) before processing to the amidoximation of the sorbent. This material is expected to combine several advantages: (a) renewable resource, for the coating layer, (b) fast kinetics, associated to the size of sorbent particles, (c) easy solid/liquid separation, due to the magnetic core, and (d) high reactivity, brought by the functionalization of chitosan with amidoxime groups. The material is characterized by FTIR and SEM-EDX analysis, titration (for N content determination), pH_{ZPC} determination, X-ray diffraction analysis, and thermal analysis. The sorption properties for U (VI) and Eu(III) (representative of rare earth element family, REEs) are tested in batch systems for selecting optimum pH, analyzing uptake kinetics and sorption isotherms. The effect of pH on the selective separation of U(VI) from Eu(III) from binary solutions is also investigated. Finally, desorption properties are investigated using HCl solutions: desorption kinetics is tested as well as the recycling of the sorbent. Uranyl and Eu(III) have been selected as representative elements present in the leachates produced during the processing of low-grade Egyptian ores. In the last part of the work, the recovery of uranium from real ore leachate is tested using this magnetic amidoxime resin.

2. Materials and methods

2.1. Materials

Chitosan (deacetylation degree: 90.5%), malononitrile and sodium hydride were supplied by Sigma-Aldrich (Taufkirchen, Germany) and were used as received without purification. Dry dimethylformamide, methanol and epichlorohydrin were purchased from Fluka AG (Buchs, Switzerland). Source of metal ions (i.e., uranyl sulfate, europium chloride) were obtained from Sigma-Aldrich. Stock metal solutions were prepared at the concentration of 1 g L^{-1} and were diluted with Milli-Q water, at fixed pH value, just before use. The pH of U(VI) solution was adjusted using 0.1/1 M H_2SO_4 and NaOH solutions; while for Eu(III) solutions the pH was controlled using 0.1/1 M HCl (or 0.1/1 M H_2SO_4) and NaOH solutions. Other reagents were supplied by Prolabo (VWR, Fontenay-sous-Bois, France).

2.2. Synthesis of sorbent

2.2.1. Synthesis of magnetic chitosan micro-particles (MG-CH)

The preparation of this material was already described [60]. Briefly, the magnetite was prepared by the hydrothermal co-precipitation method, the so-called Massart method [61]. Iron(II) (6.62 g, as $FeSO_4 \cdot 7H_2O$) and iron(III) (8.68 g, as $FeCl_3$) were co-precipitated at 40 °C in the presence of chitosan (4 g dissolved in 200 mL of a 20% (w/w) acetic acid solution) by drop wise addition of NaOH (2 M) under constant stirring. The pH was controlled to 10–10.4. The reactor was then maintained under agitation for 1 h at 90 °C. The magnetic particles were recovered by magnetic separation, abundantly rinsed with demineralized water.

2.2.2. Synthesis of epichlorohydrin-activated magnetic chitosan microparticles (EPI-MG-CH)

Wet magnetic particles were mixed with an alkaline epichlorohydrin (EPI) solution (0.01 M EPI in a 0.067 M NaOH solution; i.e., pH 10). The molar ratio between epichlorohydrin and chitosan in magnetic particles was set to 1:1. The mixture was maintained under agitation for 2 h at 40–50 °C. This reaction allows cross-linking chitosan to prevent its dissolving in mild acid solutions.

In a second step, the washed material (magnetically separated) was reacted with 150 mL of 1:1 ethanol/water solution in which 15 mL of EPI was introduced. The mixture was agitated for 3 h, before being washed up of unreacted reagents with ethanol (3 times) and Milli-Q water. The solid wet material was then freeze-dried for 24 h (−54 °C, 0.1 mPa). The final product (EPI-MG-CH) is cross-linked and holds spacer arms for further chemical modification.

2.2.3. Grafting of nitrile groups (Nitrile-MG-CH)

Malononitrile (9.9 g) was added to dry dimethylformamide (DMF, 60 mL volume) before adding 3.4 g of sodium hydride. The mixture was heated to 60 ± 4 °C for 1 h. After cooling at room temperature, the dried EPI-MG-CH micro-particles were introduced in the mixture under heating (at 80 ± 4 °C) for 6 h. After magnetic separation the material was rinsed several times with DMF before being rinsed with Milli-Q water and air-dried.

2.2.4. Amidoximation of the sorbent (AM-MG-CH)

First, a hydroxylamine solution was freshly prepared by dissolving of 21 g of hydroxylamine hydrochloride in 150 mL of 5:1 methanol/water solution. The pH of the mixture was controlled to 9–10 using 5 M NaOH solution for the neutralization of hydroxylamine. The precipitate of NaCl was removed by filtration [62].

The hydroxylamine solution was reacted with Nitrile-MG-CH solid at 75 ± 2 °C for 2 h under constant stirring. After magnetic separation the sorbent was rinsed several times with methanol/water solution before being freeze-dried overnight [29].

2.3. Characterization of sorbent

SEM (scanning electron microscopy) observations were performed on a quanta FEG 200 (FEI France, Thermo Fisher Scientific, Mérignac, France) and the EDX (energy dispersive X-ray) analysis was obtained using an Oxford Inca 350 (Oxford Instruments France, Saclay, France) coupled to SEM equipment. The raw sorbent was first analyzed and then compared with the sorbent after metal sorption (Eu(III), U(VI) and Eu(III) + U(VI)), and after metal desorption.

X-ray diffraction patterns were obtained using a Philips PW 3710/31 diffractometer (PANalytical B.V., Almelo, The Netherlands), equipped with a scintillation counter, a Cr-target tube and a Ni filter at 40 kV and 30 MA. Spectra were compared with PDF-2 database for mineral identification.

The thermogravimetric analysis was performed using TGA-50/DTA-50/DTG-50 Shimadzu thermogravimetric analyzer (Shimadzu Scientific Instruments, Kyoto, Japan). Analyses were performed under N_2 atmosphere, with a ramp of temperature of 10 °C min^{-1}.

Infra-red spectra (FTIR) were obtained in the wavenumber range 4000–400 cm^{-1} using a VERTEX70 spectrometer (Bruker, Ettlingen, Germany) equipped with a FTIR-ATR (attenuated total reflectance tool). Materials were analyzed at the different stages of the synthesis process. In addition, the spectra were compared for the raw material, after Eu(III), U(VI) sorption and after metal desorption in order to identify the reactive groups that were involved in metal binding but also to evaluate the possible degradation of chemical groups during the sorption/desorption cycle.

Elemental analysis was carried out using a CHONS elemental analyzer (Vario EL III, Elemental Analyzer, Langenselbold, Germany).

The pH-drift method was used for the determination of the pH of zero charge (pH_{ZPC}) [63]. A series of solutions was prepared with pH varying between 1 and 11 using NaCl as the background salt (at the concentration of 0.1 M). The material was shaken for 48 h with the different solutions with a sorbent dosage of 2 g L^{-1}. The sorbent was magnetically separated from the solution and the equilibrium pH was measured using a Cyber Scan pH 6000 pH-meter (Eutech Instruments, Nijkerk, The Netherlands). The equilibrium pH was measured and compared to the initial pH value (ΔpH). The pH_{ZPC} is defined by: ΔpH = 0.

2.4. Sorption and desorption procedures

Sorption studies were performed in batch systems. The solutions (volume: V, L) were mixed with the sorbent particles (amount: m, g) using a reciprocal shaker at the velocity of 150 rpm. The pH was not adjusted during the sorption step but was systematically measured at the end of the experiments. The sorbent dosage (SD, SD = m/V) was varied for the different experiments. The temperature was T: 20 ± 1 °C. The contact time was 48 h, except for uptake kinetics, where samples were collected at fixed contact times (agitation was provided by a jar-test agitator at the velocity of 210 rpm). The initial concentration (C_0: mg L^{-1} or mmol L^{-1}) was set in the range 40–60 mg metal L^{-1} (except for sorption isotherms where the initial metal concentration was varied between 5 or 15 mg L^{-1} and 350 mg L^{-1}). Samples were magnetically-treated for separating the sorbent from the solution; the residual concentration in the solution (C_{eq} or C(t), mg L^{-1} or mmol L^{-1}) was analyzed by ICP-AES (inductively coupled plasma atomic emission spectrometry). The mass balance equation was systematically used for calculating the sorption capacity (q_{eq} or q(t), mg g^{-1} or mmol g^{-1}): $q = (C_0 - C) \times V/m$.

In order to evaluate the selectivity of the sorbent for U(VI) and/or Eu(III) as a function of the pH, a series of equimolar binary solutions (0.4 mmol L^{-1}) were prepared at pH_0: 1, 2, 3, 4 and 5. The sorbent dosage was set to 300 mg L^{-1}. The solutions were maintained under agitation for 24 h. After magnetic separation, the pH was analyzed and the residual concentrations were determined by ICP-AES. The sorption capacities were determined by the mass balance equation and the distribution coefficient, K_d (L g^{-1}), was determined by the ratio q_{eq}/C_{eq}. The selectivity coefficient ($SC_{M1/M2}$) was determined by:

$$SC_{M1/M2} = \frac{K_d(M1)}{K_d(M2)} \quad (1)$$

For the study of metal desorption, the kinetics were performed using the sorbent samples loaded with metal ions during the uptake kinetics. The metal-loaded sorbent was magnetically separated, rinsed with water before being shaken with 0.5 M HCl solution (SD: 300 mg L^{-1} for U(VI) and 250 mg L^{-1} for Eu(III)). Samples were collected and analyzed by ICP-AES for evaluating metal release. The recycling of the sorbent was tested for five successive cycles of sorption/desorption. The sorbents were loaded with U(VI) and Eu(III) solutions (C_0: 187 mg U L^{-1} at pH 4 or 236 mg Eu L^{-1} at pH 5) using a sorbent dosage of 0.5 g L^{-1} (agitation time 24 h). For the desorption steps the contact time was set to 2 h and the sorbent dosage was fixed to 1.27 g L^{-1} using 0.2 M HCl solutions as the eluent. Residual metal concentrations in the solution and in the eluate were analyzed by ICP-AES. The mass balance equation served to evaluate the sorption and desorption efficiencies.

2.5. Modeling of uptake kinetics and sorption isotherms

The uptake kinetics are controlled by the intrinsic reaction rate, which can be modeled using the conventional pseudo-first order reaction rate (PFORE) [64], and the pseudo-second order reaction rate (PSORE) [65]. These equations, initially developed for describing homogeneous chemical reactions, have been widely used for modeling uptake kinetics. The rate coefficients are apparent constants that integrate the contribution of the mechanisms of resistance to diffusion. Indeed, in addition to the proper reaction rate, the kinetic profiles should also take into account the effects of resistances to bulk diffusion, film diffusion and intraparticle diffusion [66]. In the case of microparticles, the small intraparticle depth limits the effect of resistance to intraparticle diffusion on kinetic control. This will be verified below. Table AM1 (see Additional Material Section) reports the PFORE and PSORE equations. The parameters were evaluated using a non-linear regression method (and Mathematica® facilities, Wolfram, Paris, France) and the quality of the fit was measured by the estimated variance (EV) and the determination coefficient (R^2).

Sorption isotherms represent the distribution of the solute (i.e., metal ions) between the solid and the liquid phases at equilibrium and at constant temperature. This is represented by the plot of the sorption capacity, q_{eq} (mmol g^{-1}), vs. the residual metal concentration, C_{eq} (mmol L^{-1}). Many equations have been designed for modeling sorption isotherms [66]; however, the most frequently used are the mechanistic equation described by Langmuir [67], the empirical equation of Freundlich [68], and the Sips equation that combines both Langmuir and Freundlich equations. Table AM2 (see Additional Material Section) reports the mathematical equations that correspond to these three models. The specific parameters of these models have been also determined by non-linear regression.

2.6. Application to metal recovery from alkaline leachate of sedimentary Egyptian ore

The sorption process was applied to alkaline leachates of dolostone-based ore material extracted from El Alluga area (East of Abu Zeneima, southwestern Sinai, Egypt). The mineral composition of the ore is reported in Table AM3 (see Additional Material Section). This ore is part of a sedimentary geological basin; the ore is mainly constituted of dolomite, pyrite, chalcosite, malachite (CuS), chalcopyrite, sklodowskite and torbernite. Associated minerals containing copper, iron, manganese, iron, uranium, thorium, zirconium (as zircon), baryum (as barite) and titanium (as titanite, or sphene) are also present as traces. Several leaching agents have been tested, including acid and alkaline solutions (See Additional Material Section). However, most competitive leaching was obtained using carbonate/bicarbonate leaching (120 kg of carbonate and 20 kg of bicarbonate per ton, in the presence of potassium permanganate, 2 kg per ton). The S/L ratio was set to 1:2 and the slurry was maintained under agitation for 6 h at 60 °C. The leaching efficiency reached 79.3 ± 1% for U(VI). Table AM4 (see Additional Material Section) shows the composition of the alkaline leachate; the initial pH was close to 10.54. The treatment of 3 kg of ore produced 5.34 L of leachate.

The recovery of target metal ions was performed in batch system under agitation for 5 h by mixing 1 g of sorbent with 1 L of solution at the temperature of 25 ± 2 °C. The pH of the solutions was controlled to 2–5 using sulfuric acid solutions.

3. Results and discussion

3.1. Characterization of sorbent

3.1.1. FTIR characterization

The synthesis of the sorbent is summarized in Scheme 1. Magnetic chitosan particles, after being activated with epichlorohydrin, are reacted with malononitrile. In the last step (the amidoximation) nitrile groups are modified. As a consequence several markers can be used to follow the progress of the reaction, using for example FTIR spectrometry (Fig. 1 and Table 1): (a) the incorporation of magnetite core, by the appearance of Fe-O band; (b) the appearance of C-Cl signal on EPI-MG-CH (epichlorohydrin activated magnetic chitosan), (c) the appearance of nitrile groups, after reaction with malononitrile (Nitrile-MG-CH), (d) the disappearance of nitrile groups and the appearance of amidoxime groups (AM-MG-CH). The wide band around 557–559 cm^{-1} clearly demonstrates the presence of magnetite in the composite material: this band is assigned to Fe-O stretching bond. The appearance of a small band at 808 cm^{-1} on EPI-MG-CH confirms that epichlorohydrin has effectively reacted with chitosan; indeed this band is attributed to the stretching vibration of CH_2-Cl bond. The disappearance of this band with further reaction with malononitrile confirms that the substitution is quantitative. The grafting of malononitrile is demonstrated by the appearance of a strong band at 2362 cm^{-1}, which is assigned to the stretching vibration of nitrile (C≡N bond). This typical band completely disappears after the amidoximation reaction: the reaction is again quantitative. The presence of a peak at 932 cm^{-1} corresponding to −C═N−OH bond was reported for the amidoximation of chitosan [69]; this band does not appear in Fig. 1. It is noteworthy that the band at 1648 cm^{-1}, assigned to C═N stretching in secondary amide bond, is shifted to lower wavenumber, close to 1614 cm^{-1}, after amidoximation: this was interpreted as the modification of the environment of amine functions due to the interaction of −C═N- bond with $-NH_2$ bond.

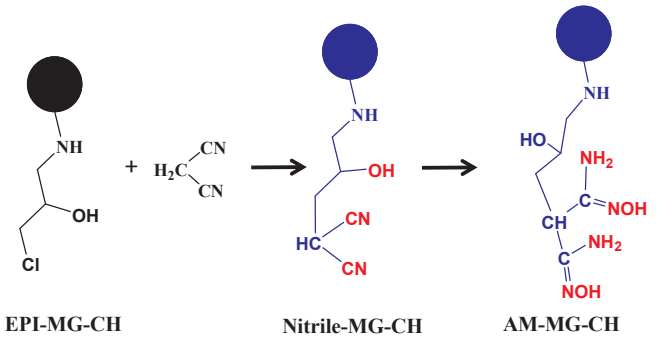

Scheme 1. Reaction pathway for the synthesis of the sorbent (epichlorohydrin activated magnetic chitosan (EPI-MG-CH) → malononitrile-grafted magnetic chitosan (Nitrile-MG-CH) → amidoxime functionalized magnetic chitosan (AM-MG-CH)).

Fig. 2 and Table 2 show, respectively, the FTIR spectra and band assignments of the raw sorbent, after metal sorption (either Eu(III) and U(VI)) and after metal desorption. After metal sorption the C═N stretching bond is shifted toward higher wavenumbers (from 1614 cm^{-1} to 1625 or 1648 cm^{-1}, for Eu(III) and U(VI), respectively), while after metal desorption the wavenumber is dropped back to 1602 cm^{-1}. This means that this band, which is associated to amidoximation, is affected by metal binding and restored when the metal is removed from the sorbent. This is consistent with the study of uranyl sorption of amidoximated chitosan/poly(acrylonitrile) sorbent [69]. In addition, the band at 1151 cm^{-1} (associated to the convolution of the vibrations of C−N stretching bond and C−O stretching bond) is considerably reduced after metal binding and is restored after metal desorption. This means that amine groups and C−O groups in the amidoxime environment are also involved in metal binding.

3.1.2. Elemental analysis

The elemental analysis of the nitrile-chitosan derivative shows the relative percentages: 23.03%, 3.66% and 6.98% for C, H and N, respectively. This corresponds to a nitrogen content of about 4.98 mmol N g^{-1}. After the amidoximation of the composite the percentages vary to 22.9%, 5.11% and 11.02, respectively. The substantial increase in nitrogen content clearly demonstrates the efficiency of the amidoximation reaction: the nitrogen content is close to 7.87 mmol N g^{-1}. This means that the substitution of nitrile groups reaches about 58%. The titration of the sorbent reveals that the nitrogen-based functions represent about 6.91 mmol −NH g^{-1}; this is slightly lower than the value of nitrogen deduced from elemental analysis. This can be explained by the fact that some nitrogen appearing in specific functional groups (such as −C(═NOH)) are not titrated as amine groups.

The weight loss at 650 °C, which was determined by calcination, shows that the polymer content in the composite represents about 61% (w/w); the remaining fraction is the magnetite material. The actual fraction of nitrogen in the polymer compartment is then 12.9 mmol N g^{-1} polymer; similarly the amine content is close to 11.33 mmol −NH g^{-1} polymer.

3.1.3. SEM observations and SEM-EDX analyses

Fig. 3 reports both the general morphology of sorbent particles and their EDX analysis (energy dispersive X-ray analysis) as raw particles, after metal sorption (alone or in combination) and after metal desorption). The general morphology is not affected by metal binding and metal desorption. The surface is irregular showing some plane surfaces entrapped in the mass of the sorbent and submicronic irregular aggregates at the surface of the materials. The size of particles ranges, in most cases (not shown), between a few microns and about 200–300 μm.

The EDX analysis confirms the presence of magnetite (Fe element) in the composite material (MG-CH) entrapped in organic coating of chitosan. EDX only allows a semi-quantitative analysis; however, the mass fraction of iron is close to 45%; this is consistent with the order of magnitude of iron in the precursors of magnetite (iron(II) sulfate and iron(III) chloride; i.e., about 4.3 g) compared to chitosan (4 g): the decrease in the mass fraction (i.e., 45% vs. theoretical value about 52%) is

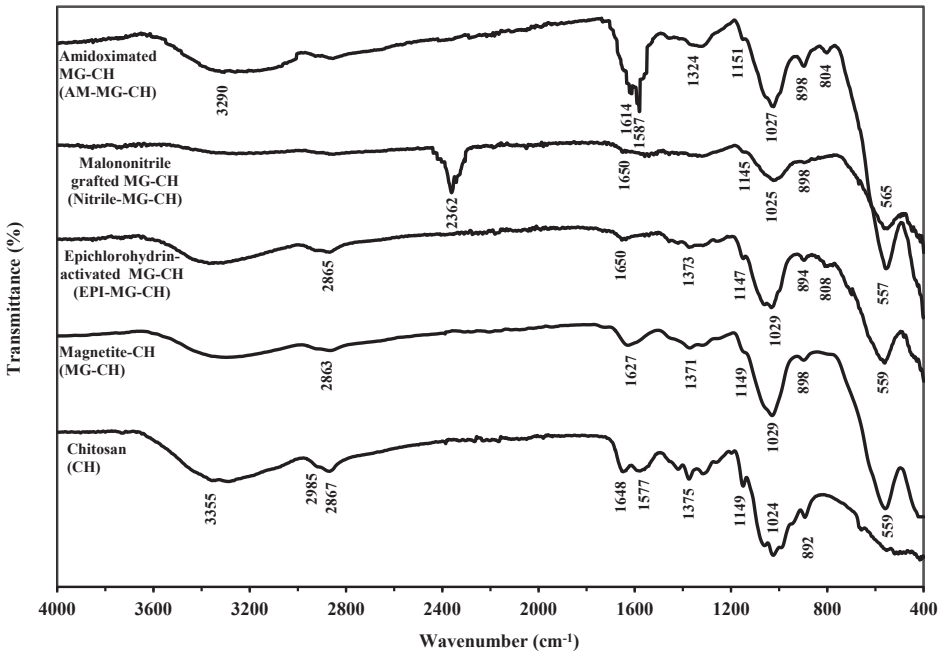

Fig. 1. FTIR spectra of the different intermediary products in the synthesis of amidoxime-functionalized sorbent (chitosan (CH), magnetic chitosan (MG-CH), EPI-MG-CH, Nitrile-MG-CH and AM-MG-CH).

due to the incomplete conversion of precursors into magnetite. This is also consistent with the percentage of magnetite calculated from the mass loss at 650 °C (i.e., 49%, see above). After chemical modification and grafting of organic material (amidoximated sorbent) the fraction of Fe element significantly reduces by 9%: the grafting of new reactive groups on the biopolymer logically decreases the relative fraction of inorganic fraction in the resin. The sorption of U(VI) in HCl solution solutions is followed by the appearance of the relevant peaks of U and Cl elements (atomic fraction close to 0.3%, mass fraction for U close to 4%) and a non-negligible increase in O element fraction, due to the binding of uranyl-based ions, UO_2^{2+}. Europium binding is also confirmed by the appearance of the Eu bands on EDX spectrum: the atomic fraction is again close to 0.3% (mass fraction close to 2.2%). In the case of multi-metal loaded sorbent the Cl band is not appearing and the new peaks are only U and Eu elements (with atomic and mass fractions consistent with previous data: total atomic fraction 0.26% and total mass fraction close to 3%). After metal desorption, the metal elements completely disappeared: metal desorption is highly efficient; the presence of Cl element is directly due to the use of HCl acid for metal desorption and the binding of chloride ions onto the surface of the sorbent. It is noteworthy that the final fraction of iron in the sorbent is close to 30%: this means that a fraction of magnetite was probably released due to leaching mechanism under drastic acidic conditions.

3.1.4. XRD analysis

Fig. AM1 (see Additional Material Section) shows the poorly-resolved XRD patterns of the intermediate composite (after nitrilation) and the final amidoximated sorbent. The two spectra are poorly resolved, especially compared with conventional XRD patterns of pure magnetite; the mineral compartment expected to be formed during the synthesis of the composite. The poor resolution can be directly explained by the effect of polymer coating on the crystallinity of the composite; the calcination and the thermogravimetric analyses have shown that polymer coating represent about 60–64% of the total weight of the composite. The crystallinity of the core magnetite particles is then masked leading to poorly marked peaks. Table AM6 (see Additional Material Section) reports the assignments of the peaks on the XRD patterns for these two materials and their comparison with the reference magnetite material (Fe_3O_4, magnetite mineral phase). The position of the peaks is poorly affected by the chemical modification of the polymer and the values of d-spacing are consistent with those of the reference material. This characterization, despite the poor resolution, confirms that the synthesis procedure effectively produced a magnetite core inside the particles.

3.1.5. Thermogravimetric analysis

The thermogravimetric analysis of the sorbent is characterized by 4 steps [60,70,71]:

Table 1
Assignments of bands appearing in FTIR spectra of chitosan, magnetic chitosan (MG-CH), epichlorhydrin-grafted chitosan (EPI-MG-CH), malononitrile-grafted magnetic chitosan (Nitrile-MG-CH) and amidoximated sorbent (AM-MG-CH).

Vibration	Ref.	Wavenumber range*	CH	MG-CH	EPI-MG-CH	Nitrile-MG-CH	AM-MG-CH
Overlapping of stretching of O—H and N—H bonds	[81]	3500–3000	3650–3000	3640–3050	3600–3050	3500–3200	3650–3000
Stretching of C≡N bond	[82]	2260–2222	–	–	–	2362	–
Stretching of C═N secondary amide bond	[83,84]	1690–1630	1648	1627	1650	1650	1614
Bending of primary and secondary–OH group	[82]	1420–1330	1375	1371	1373	W	1324
Stretching of C—O	[83,85]	1190–1130	1149	1149	1147	1145	1151
Stretching of primary C—N bond	[85]	1090–1020	1024	1029	1029	1025	1027
β-D-glucose unit and rocking CH_2 bond	[85–87]	890–720	892	898	894	898	898, 804
Stretching of CH_2—Cl bond	[85]	700–800	–	–	808	–	–
Stretching of Fe—O bond	[57,87,88]	556	–	559	559	565	557

* In reference.

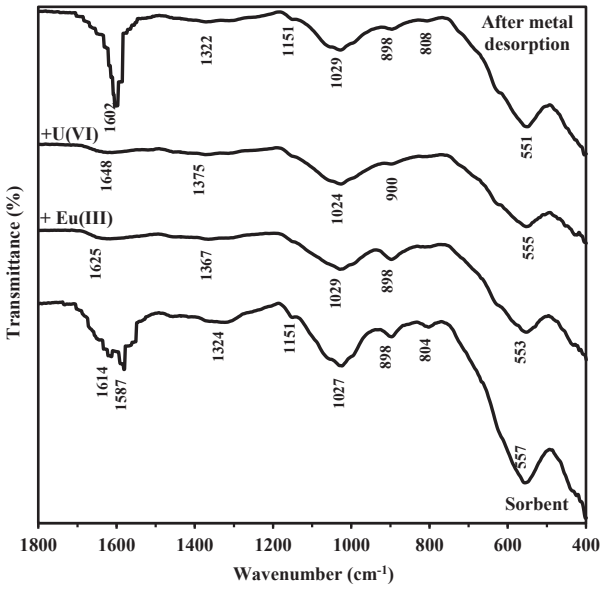

Fig. 2. FTIR spectra of the sorbent before, after Eu(III) sorption (+Eu(III)), after U(VI) sorption (+(U(VI)) and after metal desorption (wavenumber range limited to 1800–400 cm^{-1}).

(a) from 20.7 °C to 209.4 °C, the mass loss counts for about 10% and represents the loss of water absorbed on the material,
(b) from 209.4 °C to 296.6 °C, the mass loss reaches 31.2% (total cumulated mass loss: 41.2%); the dehydration of the saccharide ring and the partial depolymerization are responsible of the partial degradation of the chitosan backbone,
(c) from 296.6 °C to 600.7 °C; the mass loss is close to 18.8% and this is attributed to the degradation of the organic skeleton, including the degradation of amine compounds and relevant functional groups,
(d) from 600.7 °C to 801.8 °C, the mass loss counts for 9.1%; this is assigned to the final degradation of the remaining organic materials and the phase change of magnetite core.

The total weight loss at 801.8 °C represents 69.1%; this is little higher than the weight loss observed in calcination of the composite material at 650 °C (i.e., 61.1%); this is due to the difference in the mode of thermal degradation (aerobic vs. anaerobic thermal degradation) and the higher temperature that may affect the phase transition of the mineral core.

3.1.6. Determination of pH_{ZPC}

The pH-drift method was used for evaluating the pH_{ZPC} of the sorbent (Fig. 4). The pH variation between the initial and final values increases from pH 1 to pH 4 (reaching a maximum value, ΔpH, close to +2.5) and then sharply decreases till pH 8 (where the ΔpH is close to 0): the pH_{ZPC} is close to 8.13. Above pH 8.13 the ΔpH becomes negative: the residual pH decreases. These strong pH variations show that the sorbent is highly reactive with protons from the solution. This also means that below pH 8 the sorbent will be mainly positively-charged while theoretically above pH 8 the sorbent will be negatively charged. Due to the intrinsic hydrolysis of metal ions at high pH values and the occurrence of precipitation phenomena the sorption study is limited to pH values below 6 and then it is possible considering that in the whole pH range of this study the sorbent will be exclusively positively-charged. This may be important for anticipating on the sorption efficiency and the mechanisms involved in metal binding. This value is significantly higher than the value cited for poly(acrylonitrile)/amidoxime/bentonite composite (i.e., 6.3) [38], for amidoxime-functionalized hydrothermal carbon support (i.e., 4.7) [72] or for amidoximated polyacrylonitrile/montmorillonite composite (i.e., 4.3) [73]. On the other hand, in the case of algal biomass functionalized with amidoxime, the pH_{ZPC} was found close to 10.0 [74]; this is close to the value found for MCM-41 silica decorated with poly(acrylonitrile) and further functionalized by amidoxime (i.e., close to 10.5) [75]. The environment of amidoxime groups sounds to have a great influence on the charge hold by the sorbent.

3.2. Effect of pH

The pH may influence the charge of sorbent particles: though in the pH range investigated in this study the sorbent is positively-charged, the lower the pH the higher the protonation of the sorbent and the higher is the concentration of counter-anions. In addition, the pH can influence the speciation of metal ions due to the formation of hydrolyzed species or complexes associated to the counter ions brought by the salt or the acid used for pH control. In the case of Eu(III), with pH controlled with sulfuric acid solutions, the chemistry of metal ions is relatively simple: whatever the pH, metal ions are cationic. At pH above 3, free Eu(III) and $EuSO_4^+$ species are equally present. At pH below 3, europium is predominantly appearing as free Eu^{3+} though some other species may coexist such as $EuCl_2^+$ (whose fraction progressively decreases and disappears at pH 2) and $EuSO_4^+$ (the concentration continuously increases) (Fig. AM3, see Additional Material Section). In the case of uranyl the speciation is much more complex: the predominant species strongly change with the pH range (Fig. AM4, see Additional Material Section). Between pH 1 and 2, sulfate species (mainly neutral aqueous UO_2SO_4, and, much less, the anionic disulfate species: $UO_2(SO_4)_2^{2-}$) represent above 75% of uranyl in solution; remaining species are free uranyl ions. Between pH 2 and 3.5–4, the fraction of free uranyl species progressively increases up to 75%, while sulfate species tend to disappear (at pH above 5). Above pH 4, the contribution of free uranyl species drastically decreases being progressively replaced by polynuclear hydrolyzed species (mainly $(UO_2)_3(OH)_5^+$, $(UO_2)_4(OH)_7^+$, $(UO_2)_2(OH)_2^{2+}$) and to a lower extent by $(UO_2)OH^+$.

Fig. 5a shows that Eu(III) sorption progressively increases with the

Table 2
Assignments of bands appearing in FTIR spectra of sorbent: raw material, after Eu(III) sorption, after U(VI) sorption and after metal desorption.

Vibration	Ref.	Wavenumber Range*	Sorbent	Eu(III) Sorption	U(VI) Sorption	After metal desorption
Overlapping of stretching of O—H and N—H bonds	[81]	3500–3000	3650–3000	3750–3000	3780–3000	3450–3000
Stretching of C=N bond (secondary amide)	[83,84]	1690–1630	1614	1625	1648	1602
Bending of O—H bond	[82]	1420–1330	1324	1367	1375	1322
Stretching of C—N bond (secondary amine) and stretching of C—O bond	[83,85]	1190–1130	1151	W	W	1151
Antisymmetric stretching of C—O—C bond and stretching of C—N bond (primary amine)	[57,85–89]	1090–1020	1027	1029	1024	1029
β-D-glucose unit and rocking of CH_2 bond	[85–87]	890–720	898, 804	898	900	898, 808
Stretching of Fe—O bond	[57,87,88]	556	557	553	555	551

* In reference.

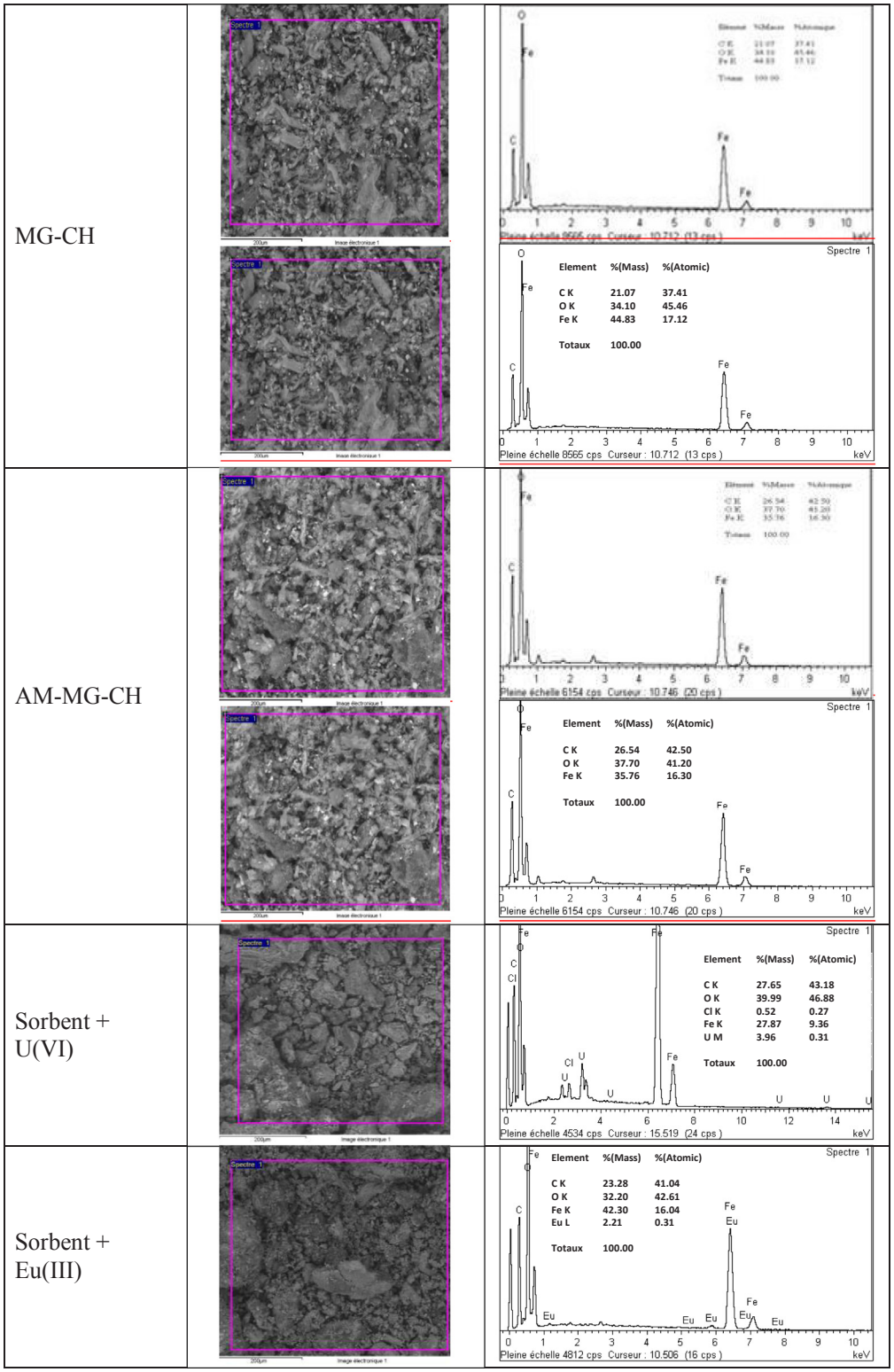

Fig. 3. SEM & SEM-EDX characterizations (scale: bar represents 200 μm).

pH: this increase is almost linear between pH 2.3 and 6. At acidic pH, the strong protonation of amine groups on amidoxime reactive groups makes difficult the binding of metal cations due to the repulsion of cationic species. When the pH increases this repulsion effect progressively decreases facilitating metal binding through chelation on amidoxime groups. Chelation of rare earth is expected to proceed through the simultaneous interaction of the metal ion with amine groups (RR′C−NH_2, with R′: =N−OH)) and O on the hydroxyl group (RR″C=N−OH, with R″: NH_2) on the amixodime functional group [29]. The deprotonation of amine groups improves the chelating ability of the material for free Eu(III) species.

For uranyl ions the pH effect is significantly different: the sorption capacity drastically increases between pH 2.3 and pH 4, between pH 4 and 5 the sorption is stabilized, while above pH 5 the sorption capacity tends to decrease. Fig. AM5a (see Additional Material Section) shows the sorption efficiency as a function of equilibrium pH: between pH 4

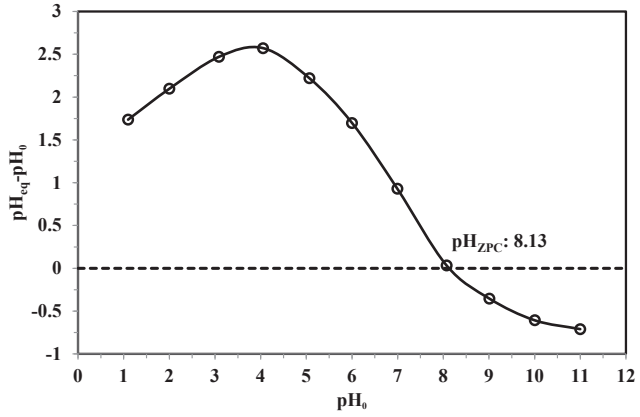

Fig. 4. Determination of pH_{ZPC} by the pH-drift method (sorbent dosage, SD: 2 g L^{-1}; background salt: 0.1 M NaCl; contact time: 48 h).

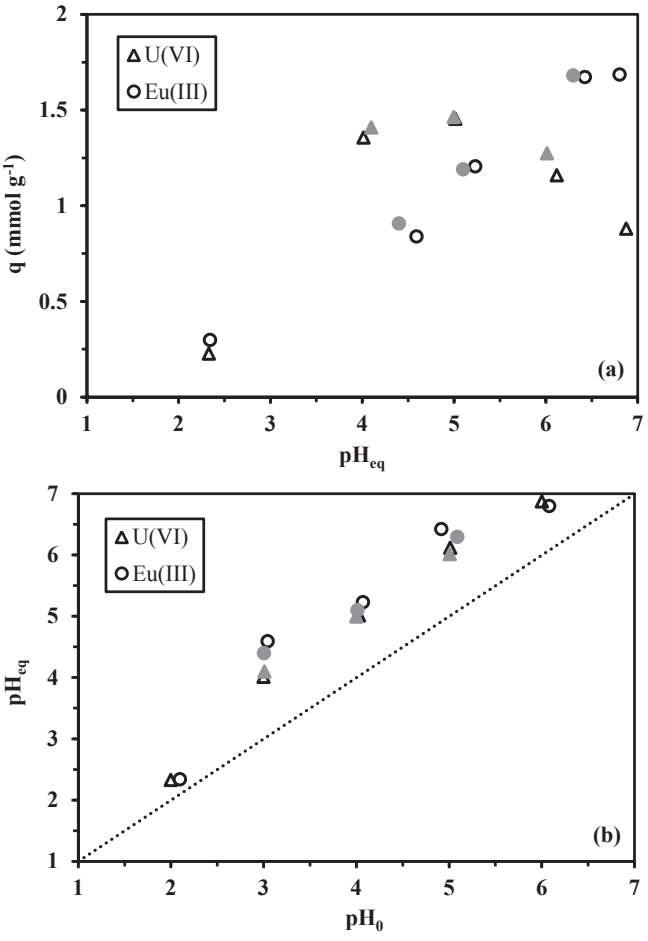

Fig. 5. Effect of pH on U(VI) sorption using amidoxime-functionalized magnetic chitosan micro-particles: (a) sorption capacity, (b) pH variation (sorbent dosage, SD: 0.2 g L^{-1}; C_0: 0.256 mmol U L^{-1} or 0.355 mmol Eu L^{-1}; contact time: 48 h).

and 5 uranyl sorption is almost complete: the reported stabilization of sorption capacity is thus relative under selected experimental conditions. However, the decrease in sorption capacity while approaching neutral conditions is confirmed by the repetition of experimental points using a second sample of sorbent: grey points represent the data obtained with the second lot; the sorption properties are remarkably similar. The progressive increase in sorption properties can be directly correlated to the predominance of free uranyl species, while the decrease in sorption performance at pH above 5 is probably associated to the progressive appearance of strongly hydrolyzed complexes. A similar profile for pH-sorption efficiency was reported for uranyl sorption using amidoximated poly(acrylonitrile)/montmorillonite composite [73]. For uranyl binding several mechanisms were proposed: (a) binding of uranyl through direct interaction of U with both the nitrogen and the oxygen of oxime group (C═N−OH, after deprotonation of hydroxyl group) [73]; (b) binding of uranyl ions through 4 different O on OH groups from vicinal amidoxime functions [76]; (c) interaction with nitrogen from amine group and from oxime group [77]; (d) formation of a “ring structure” through interactions of uranyl ions with adjacent amidoxime groups with simultaneous bonds between uranyl cation and nitrogen from amine groups and oxygen from oxime groups [72,78]. The interaction of the multidentate ligand with uranyl species is facilitated when free uranyl species predominate in the solution.

Fig. AM5b (see Additional Material Section) shows the logarithmic plot of the distribution coefficient (K_d, L g^{-1}, defined as the ratio q_{eq}/C_{eq}) as a function of equilibrium pH. In ion-exchange and solvent extraction processes involving proton exchange the slope of the plot is usually employed for evaluating the proton exchange ratio. This approach is not directly applicable for chelation mechanisms. However, in the case of Eu(III) slope close to 0.67 is observed for the pH range between 4 and 7. For U(VI) it is not possible detecting a trend, this is obviously strongly affected by the continuous change in metal speciation and the formation of hydrolyzed species.

Fig. 5b shows the pH variation during metal sorption. The equilibrium pH is usually increased by 1 pH unit; except at pH 2, where the pH variation is limited to 0.2–0.3 pH unit. This can be directly correlated to the pH variation observed in the pH-drift method for the determination of pH_{ZPC} (Fig. 4): in metal-free solutions the pH variation reached up to 2.5 pH units. This is important since a pH increase may cause metal precipitation phenomena, especially for uranyl species. For this reason for further studies the pH was set around pH 5 for Eu(III) and to pH 4 for U(VI).

3.3. Uptake kinetics

The small size of sorbent particles (below 300 μm) limits the contribution of resistance to intraparticle diffusion on the control of uptake kinetics. This is clearly supported by the observation of the kinetic profiles (Fig. 6). Under selected experimental conditions, a contact time of 60 min is sufficient for achieving more than 95% of total sorption. The fractional approach to equilibrium (FATE, not shown) shows that 65% of equilibrium sorption is achieved within 20 min for U(VI) and as low as 5 min for Eu(III). Fig. 6 also shows the modeling of experimental data with the PFORE and the PSORE; Table 3 summarizes the rate coefficients and the statistical data on the model fits. The two models show very similar determination coefficients, the estimated variances (EVs) are slightly lower for the PSORE and the comparison of the sorption capacities at equilibrium for experimental and calculated values are of the same order of magnitude. It is thus difficult selecting between the two models for fitting experimental profiles.

Both k_1 and k_2 (apparent rate coefficients for PFORE and PSORE, respectively) are about 3 times higher for Eu(III) than for U(VI); this is consistent with the FATE observations (see above). Experimental conditions selected for these kinetic experiments are little different for the two metal ions. For U(VI) the sorption capacity at equilibrium approaches 1.4 mmol U g^{-1}, which is close to 1.5 mmol U g^{-1} that corresponds to the maximum sorption capacity obtained with sorption isotherms (see below). On the opposite hand, for Eu(III) the sorption capacity at equilibrium for kinetics is much lower than the maximum sorption capacity obtained for isotherm: 1.65 mmol Eu g^{-1} vs. 2.47 mmol Eu g^{-1}. This may affect the interpretation of kinetic behaviors: the approach of the saturation of reactive groups hinders the sorption of new metal ions. In any case, the uptake kinetics shows that metal sorption is very fast, making full profit of the small size of sorbent particles.

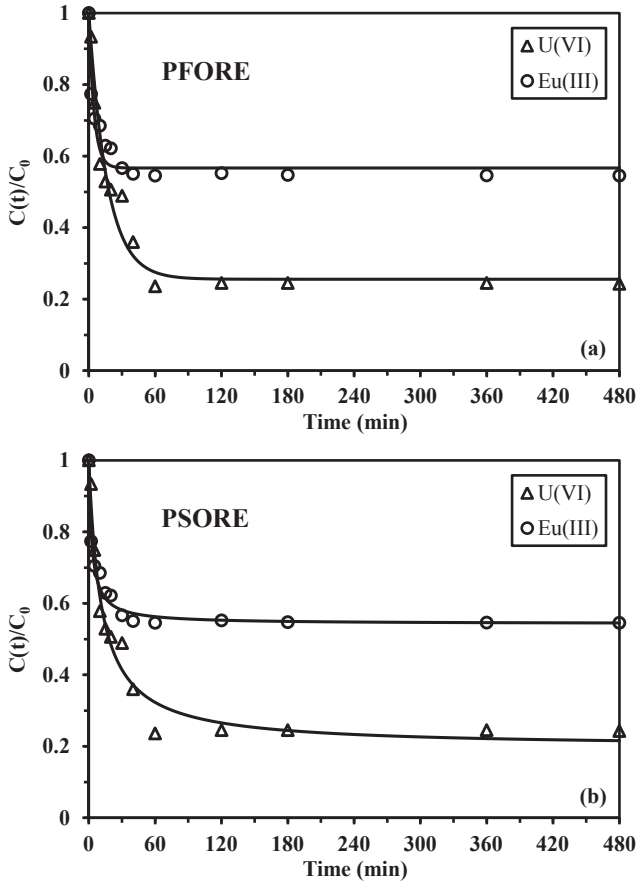

Fig. 6. Uptake kinetics for the sorption of U(VI) and Eu(III) using amidoxime-functionalized magnetic chitosan micro-particles- Modeling with the PFORE (a) and the PSORE (b) (sorbent dosage, SD: 0.1 g L^{-1}; C_0: 0.187 mmol U L^{-1} or 0.362 mmol Eu L^{-1}; pH_0: 4.0 for U(VI) and 5.1 for Eu(III)).

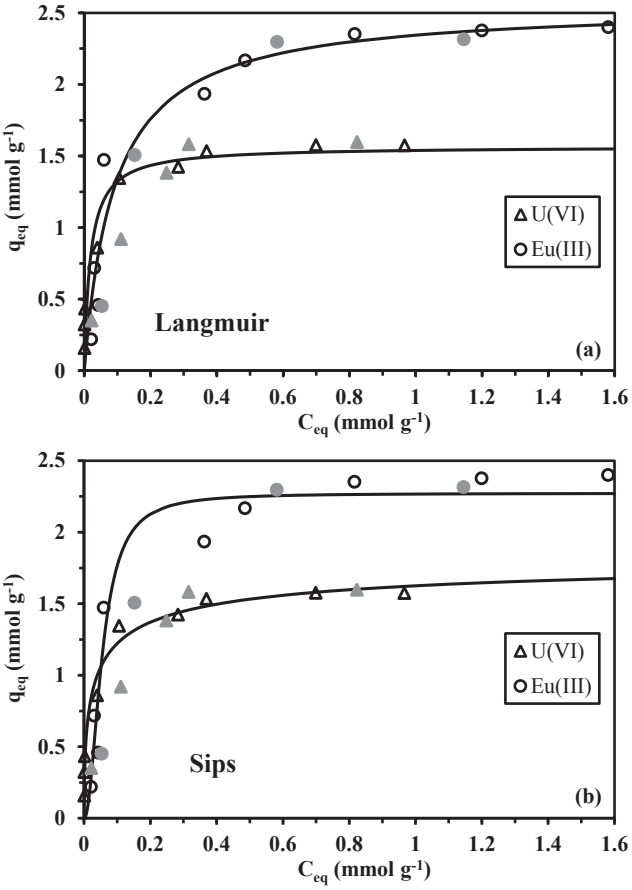

Fig. 7. Sorption isotherms for the recovery of U(VI) and Eu(III) using amidoxime-functionalized magnetic chitosan micro-particles – Modeling with the Langmuir equation (a) and the Sips equation (b) (grey symbols are comparative data obtained with a second stock of sorbent; SD: 0.2 g L^{-1}; C_0: 0–1.5 mmol U L^{-1} or 0–2.5 mmol Eu L^{-1}; pH_0: 4.0 for U(VI) and 5.0 for Eu(III); contact time: 48 h).

3.4. Sorption isotherms

The sorption isotherms are reported on Fig. 7. The curves are characterized by a steep increase in the sorption capacity at low residual metal concentration (below 0.2 mmol L^{-1}), while a saturation plateau is reached at residual concentration close to 0.4–0.6 mmol L^{-1}. The saturation plateau is consistent with the asymptotic form of the Langmuir and the Sips equations and opposite to the power-type function defined by the Freundlich equation. It is thus expected that the Freundlich equation does not correctly fit experimental data, compared to the other models. This is confirmed by Table 4 that summarizes the parameters of these models (and the statistical data analysis of mathematical fits). For Freundlich equation the determination coefficients and the EVs are worse than those obtained with the Langmuir and the Sips equations. The comparison of the Langmuir and the Sips equation is less evident: statistical parameters are very close; introducing an additional parameter in the Sips equation offers the possibility to improve the mathematical fits, at the expense of a loss in the physical significance of the model. The benefit in mathematical modeling is not sufficient for preferring this model to the mechanistic Langmuir model: in Fig. 7 the Langmuir and the Sips fits are superimposed to the experimental data; the Freundlich fit appears in Fig. AM6 (see Additional Material Section). The grey symbols in Fig. 7 represent additional data obtained with the second lot of sorbent: the experimental data are superimposed showing that the synthesis of the sorbent is successfully repeatable.

The Langmuir maximum sorption capacities (i.e., 1.57 mmol U g^{-1} and 2.56 mmol Eu g^{-1}) are consistent with the experimental saturation values (i.e., 1.50 mmol U g^{-1} and 2.47 mmol Eu g^{-1}). This is another evidence of the appropriateness of the Langmuir equation for modeling sorption isotherms. Frequently, the Sips equation allows improving the fit of experimental data in the zone of higher curvature of the sorption isotherms; this is not obvious in the present case. In the case of Eu(III) the metal speciation is not influenced by the pH (Fig. AM3, see Additional Material Section) neither the metal concentration because

Table 3
Uptake kinetics for the recovery of U(VI) and Eu(III) using amidoxime functionalized magnetic chitosan microparticles – parameters of PFORE and PSORE models (Fig. 6).

Metal ion	$q_{eq,exp.}$	PFORE				PSORE			
		$q_{eq,1}$	$k_1 \times 10^2$	EV × 10^2	R^2	$q_{eq,2}$	$k_2 \times 10^2$	EV × 10^2	R^2
U(VI)	1.413	1.389	6.06	0.89	0.968	1.450	6.01	0.65	0.968
Eu(III)	1.645	1.569	21.2	2.02	0.925	1.657	21.7	0.58	0.925

q_{eq}: mmol g^{-1}; k_1 (min^{-1}), k_2: L mmol^{-1} min^{-1}.

Table 4
Sorption isotherms for the recovery of U(VI) and Eu(III) using amidoxime functionalized magnetic chitosan microparticles – Parameters of Langmuir, Freundlich and Sips equations (Fig. 7).

Model	Parameter	Metal ion	
		U(VI)	Eu(III)
Experimental	$q_{m,exp}$	1.50	2.47
Langmuir	$q_{m,L}$	1.567	2.557
	b_L	53.86	11.03
	EV × 10^2	2.56	6.13
	R^2	0.966	0.932
Freundlich	K_F	1.771	2.338
	n_F	4.56	3.22
	EV × 10^2	2.52	13.2
	R^2	0.957	0.854
Sips	$q_{m,S}$	1.882	2.272
	b_S	6.34	402.5
	n_S	1.87	0.485
	EV × 10^2	0.78	6.32
	R^2	0.982	0.939

q_m: mmol g^{-1}; b: L $mmol^{-1}$, k_F: $mmol^{1-1/n} L^{1/n} g^{-1}$; n: dimensionless.

europium does not form polynuclear species. Metal sorption is followed by pH increase, the predominating species will not be affected and the influence of metal speciation is not expected to play a significant role in the interpretation of sorption profiles. For U(VI) the scenario is completely different: pH variation and change in metal concentration drastically change metal speciation (Fig. AM7, see Additional Material Section). At initial pH value (i.e., pH 4) free uranyl species and neutral uranyl sulfate predominate in the solution in the whole range of concentration, when the pH increases with metal sorption, the predominant species completely changes with increasing formation of polynuclear species, which are less favorable to metal sorption because of ionic charge and steric hindrance associated to the size of polynuclear hydrolyzed species.

The density of reactive groups on the composite sorbent (i.e., 7.87 mmol N g^{-1} and 6.91 mmol −NH g^{-1}) can be compared to the sorption capacities for U(VI) and Eu(III) (i.e., 1.5 mmol U g^{-1}; and 2.47 mmol Eu g^{-1}, respectively). The molar ratios (−NH)/U(VI) and (−NH)/Eu(III) at saturation of the sorbent are 4.61 and 2.79, respectively. The steric hindrance may affect the accessibility of reactive groups and their availability for matching with the geometry of metal species; the comparison of these molar ratios is then debatable but this tends to demonstrate that the reaction mode is different for the two metal ions.

Tables 5 and 6 reports the sorption performances of alternative materials for Eu(III) and U(VI), respectively. In the case of Eu(III), the amidoximated sorbent shows the highest sorption capacities and kinetic performance comparable to most of these alternative materials. Concerning U(VI), the maximum sorption capacity (close to 1.5 mmol U g^{-1}) is comparable to the performance obtained with other chitosan derivatives but lower than the levels obtained with the most efficient sorbents such as *Sargassum* biomass (i.e., 2.35 mmol U g^{-1}) [79], amidoximated *Aspergillus niger* (i.e., 2.61 mmol U g^{-1}) or 2-picolylamine functionalized synthetic resin (i.e., 2.18 mmol U g^{-1}) [80].

3.5. Sorption selectivity

One of the objectives of this work consisted of evaluating the use of this sorbent for the possible separation of uranium from rare earths in the processing of the low-grade ores as in black shales and other materials as dolostone from Egyptian mines in Sinai. In order to investigate the selectivity of the sorbent for these metals a series of bi-component equimolar solutions (0.435 mmol L^{-1}) at different pH values has been prepared and tested for the simultaneous sorption of U(VI) and Eu(III).

Table 5
Eu(III) sorption capacities (q_m, mmol Eu g^{-1}) for selected sorbents.

Sorbent	pH	Contact time (h)	q_m	Reference
Hydrous silica	5.3	4–5	2.6×10^{-4}	[90]
Sargassum polycystum	3–5	24	0.8–0.9	[91]
Bacillus subtilis	5	48	0.15	[92]
Heulandite microfibers	5	5	0.15	[93]
Kaolinite	5	0.15	3.1×10^{-3}	[94]
Crab shell	6	1	0.33	[23]
Turbinaria conoides	4.9	1	0.91	[22]
Ce(IV)-Phosphate/PAN	2	1–1.5	1.12–1.96	[95]
Chitosan nano-particles	3	1	0.76	[26]
Chitosan	3	0.5	0.32	[27]
Diglycolamic acid/Silica	3	0.5–1	0.29	[96]
Diglycolamic acid/Polyamine matrix	3	5–6	0.18	[97]
Phosphonic-grafted polystyrene resin	6.5	0.5–1	0.81	[98]
Magnetic multiwall CNT/PAA	4.3	48	0.05	[99]
Ionic liquid impregnated CMPO resin (3 M HNO_3)	*	1	0.132	[100]
D113 cation exchange resin (−COOH groups)	6.5	n.r.**	1.99–2.35	[101]
Amidoximated-sorbent	5	1	2.47	*This work*

* Acid solution.
** n.r.: not reported.

Table 6
U(VI) sorption capacities (q_m, mmol U g^{-1}) for selected sorbents.

Sorbent	pH	Contact time (h)	q_m	Reference
Chitosan	5	24	1.33	[102]
Glutamate glucan	5	24	1.53	[102]
Chitosan/azole	3.9	1.5–2	1.6	[103]
Chitosan/amine	3.9	1.5–2	1.9	[103]
Sargassum biomass	4	1	2.35	[79]
Amberlite XAD4/Succinic acid	6.5	0.6	0.52	[104]
Phosphonic-functionalized AXAD-16 resin	6	0.1	1.66	[105]
Activated carbon	3	4	0.12	[106]
Magnetic glycidyl methacrylate chelating resin	4.5	1	1.68	[107]
Magnetic chitosan nanoparticles	5	0.6	0.18	[108]
Chitosan/tripolyphosphate beads	5	80	0.99	[109]
Amberlite CG-400	3.5	5–6	0.47*	[110]
Salicylideneimine-functionalized carbon	4.3	1	1.10	[111]
Ion-imprinted magnetic chitosan resin	5	3	0.79	[112]
Grapefruit peel	5	1.5	0.59	[113]
Sunflower straw	5	10	0.03	[114]
Phosphorus-modified poly(styrene-co-divinylbenzene) chelating resin	5	5	0.41	[115]
PVA-modified electrospun nanofiber membrane	4.5	3–4	0.71	[116]
Functionalized mesoporous carbon	4	0.1–0.3	0.41	[19]
Chlamydomonas reinhardtii	4.5	1–1.5	1.42	[25]
Cellulose-camphor soot nanofibers	6	1	1.72	[117]
Cysteine-functionalized magnetic chitosan micro-particles	3.6	1	0.42	[118]
Amidoximated *Aspergillus niger*	5	3	2.61	[119]
Amberlite IRA-402 resin	3	2	0.89	[10]
β-cyclodextrin functionalized silica gel	4.5	1	0.07	[120]
DTPA-functionalized magnetic chitosan nano-particles	5	1	0.66	[121]
2-picolylamine functionalized poly (styrene-*co*-maleic anhydride) resin	5.3	2	2.18	[80]
Phosphoryl-functionalized mesoporous silica gel	5	0.15	1.92	[122]
Amidoximated-sorbent	4	1	1.50	*This work*

* In the presence of phosphate anions; **: n.r.: not reported.

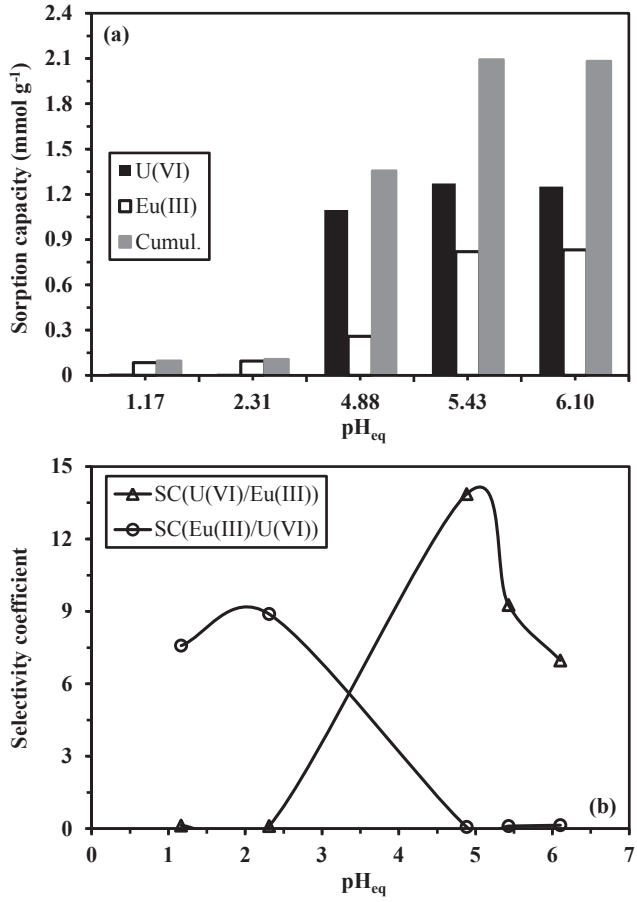

Fig. 8. Effect of pH on the selectivity of U(VI) and Eu(III) sorption from binary solutions using amidoxime-functionalized magnetic chitosan micro-particles: (a) individual and cumulative sorption capacities, (b) selectivity coefficients (C_0: 0.44 mmol U L^{-1} and 0.43 mmol Eu L^{-1}; SD: 0.25 g L^{-1}; contact time: 24 h).

Fig. 8a shows the sorption capacities of the two metal ions (together with the cumulative sorption capacity). As expected increasing the pH increased metal sorption at pH above 5, U(VI) and Eu(III) are both quite well sorbed on the amidoximated sorbent. The cumulative and individual sorption capacities are stabilized at constant value (pHs 5.4 and 6.1). At low pH values, (in the range 1.2–2.3) the sorption of uranyl ions is strongly depreciated (almost negligible) while Eu(III) maintains a weak sorption affinity. At pH close to 4.9, uranyl sorption is highly effective and much better than Eu(III) recovery. These trends are confirmed by Fig. 8b: the selectivity coefficient for U(VI) is relatively high (close to 14) at pH close to 4.9 with high sorption capacity: around 1.2 mmol U g^{-1} (this is about 80% of the sorption capacity obtained with mono-component solutions under comparable conditions), with a sorption capacity lower than 0.3 mmol Eu g^{-1} for Eu(III) (i.e., 15% of comparable sorption capacity with mono-component solutions) (Fig. 7). This means that the recovery of U(VI) can be significantly enriched on the sorbent working at pH close to 4.9. On the contrary, Eu(III) can be strongly enriched on the sorbent at pH 2.3 compared to U(VI); however, the sorption capacity remains very low (i.e., close to 0.1 mmol Eu g^{-1}).

The sorbent can be used for pre-separating the two metal ions (and probably for separating U(VI) from other rare earth elements, REEs, which have a chemical behavior close to that of Eu(III)). However, the selectivity is probably not sufficient for effectively separating these metal ions in a single step and/or in a batch mode. Playing with selective desorption, using chromatographic-based columns could contribute to improve the selective separation of U(VI) and REEs.

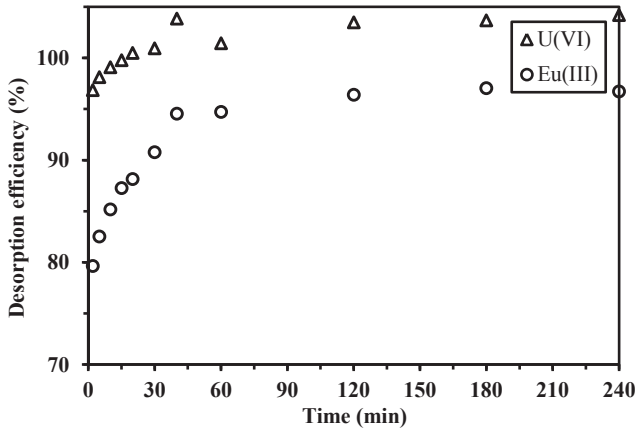

Fig. 9. Desorption kinetics using 0.5 M HCl solution (metal loaded-sorbents were recovered from uptake kinetics, Fig. 6 – Desorption: SD: 0.3 g L^{-1} for U(VI) and 0.25 g L^{-1} for Eu(III)).

3.6. Metal desorption and sorbent recycling

Hydrochloric acid solutions (0.5 M) have been used for testing metal desorption from metal-loaded sorbents. Fig. 9 shows the kinetic profiles for U(VI) and Eu(III) desorption. Uranyl desorption is complete and fast: 30 min of contact are sufficient for completely removing uranyl. On the opposite hand for Eu(III) the maximum desorption efficiency does not exceed 95% and this level of desorption is reached after 60–120 min. It is noteworthy that for U(VI) even after 2 min of contact about 96% of sorbed uranyl ions can be removed from the sorbent, while for Eu(III) the desorption efficiency does not exceed 80%. Desorption can probably be a tool for enhancing metal separation. This was not investigated in this study but it is possible suggesting to play with the pH during the sorption step and to play with contact time for the desorption step. Another way to improve the selective separation could consist of changing the eluent (testing for example carbonate/bicarbonate solutions that are efficient for eluting uranyl from conventional ion-exchange resins) and/or the concentration of HCl.

The re-use of the sorbent was also tested for five successive cycles of sorption/desorption. Table 7 summarizes these results. In the case of U (VI), under selected experimental conditions, metal recovery is highly efficient over the 5 cycles: sorption efficiency slightly decreases from 98.7% to 95.8% while desorption efficiency only decreases from 99% to 94% at the last tested cycle. In the case of Eu(III), the sorption efficiency also remains very stable, decreasing from 75.8% to 72.6% while the desorption maintains very high levels of efficiency around 99% over the 5 cycles. These results clearly establish that the sorbent can be efficiently recycled. Under selected experimental conditions, the performance of the material is maintained almost constant over 5 cycles. This makes the material highly efficient and competitive.

Table 7
Recycling of the sorbent – Sorption efficiencies and desorption efficiencies for 5 successive cycles.

Metal ion	U(VI)		Eu(III)	
Cycle #	Sorption efficiency (%)	Desorption efficiency (%)	Sorption efficiency (%)	Desorption efficiency (%)
1	98.7 ± 0.3	99.2 ± 0.4	75.8 ± 1.1	100 ± 0.5
2	98.1 ± 0.4	99.7 ± 0.3	74.5 ± 0.1	98.3 ± 0.4
3	97.6 ± 1.1	98.2 ± 1.7	74.7 ± 0.3	97.5 ± 1.9
4	96.5 ± 0.4	97.0 ± 2.6	73.8 ± 0.8	99.1 ± 1.2
5	95.8 ± 0.1	94.1 ± 0.7	72.6 ± 0.4	100 ± 2.5

Table 8
Efficiency of metal recovery using amidoximated sorbent for the processing of alkaline leachates of dolostone ores – pH effect on recovery efficiency.

Metal ion	Metal recovery (%)			
	pH 2	pH 3	pH 4	pH 5
U(VI)	10.5	48.4	66.2	64.9
Al(III)	5.9	11.8	28.3	34.8
Fe(III)	7.8	17.1	53.8	65.7
Cu(II)	7.5	18.9	59.0	65.5
Zn(II)	2.2	6.7	22.2	31.1
Ni(II)	7.3	8.4	13.7	19.0
Mn(II)	1.6	6.1	11.2	12.9
Ti(IV)	0.0	5.7	11.4	17.1
Total sorption capacity (mmol g^{-1})	0.87	2.64	5.65	6.52
Final pH	1.88	3.54	4.77	5.23

3.7. Metal recovery from alkaline leachates of dolostone ore

The application of the composite sorbent to the recovery of a series of eight metal ions present in the alkaline leaching of dolostone ore is reported in Table 8 for different pH values. The sorption efficiency increases with the pH, especially between pH 2 and pH 4; above pH 4 the sorption efficiency tends to stabilize. This is confirmed by the increase of sorption capacities with pH (not shown): in the case of U(VI) the sorption capacity increases up to 219–223 mg U g^{-1} (i.e., around 0.93 mmol U g^{-1}) at pH 4–5; this is about 38% lower than the sorption capacity obtained on synthetic pure solutions (i.e., 1.5 mmol U g^{-1}, sorption isotherms, Fig. 7). The competition effect of base metals decreases uranyl recovery. However, the total sorption capacity for selected metal ions reaches up to 5.65 mmol g^{-1} at pH 4.8, and 6.52 mmol g^{-1} at pH 5.2 (Table 8). These values are even higher than the values obtained for Eu(III) sorption isotherm. This means that base metals probably compete for the same sorption sites but can also bind to other reactive groups.

The high affinity of amidoximated sorbent for uranyl ions is confirmed: regardless of the pH, uranyl recovery is much more efficient than for other base metals. The sorption of Cu(II) and Fe(III) is also very efficient at pH 5 (comparable to the recovery of uranyl, close to 66%). At pH 3, uranyl sorption decreases but less than for other metal ions: the sorption is more selective for U(VI) at this pH value. The strict comparison is difficult since the molar concentrations are not the same in the feed solution for the different metals. The calculation of the distribution coefficients ($K_d = q/C_{eq}$; L kg^{-1}) allows a better comparison of the respective affinities. Fig. AM8 (see Additional Material Section) shows the plot of $\log_{10} K_d$ vs. equilibrium pH for the different metal ions, while Table AM5 reports the parameters of linear plots. For most of selected metal ions the log-plot exhibits a linear trend with a slope ranging between 0.28 and 0.4, while for Ni(II) a much lower slope is obtained (i.e., 0.135). The curve for U(VI) is shifted toward lower pH values; this is consistent with the greater selectivity of the sorbent for uranyl ions at low pH values.

4. Conclusion

The amidoximation of chitosan strongly improves its efficiency for the sorption of U(VI) and Eu(III) in near neutral solutions (pH 4–5). The modified sorbent exhibits one of the highest sorption capacities compared to literature (2.47 mmol Eu g^{-1}). The sorbent conditioned as magnetic micro-particles has relatively fast properties for metal sorption; the small size of sorbent particles and the thin layer of polymer on magnetite core limit the contribution of resistance to intraparticle diffusion on the control of uptake kinetics: 60–90 min are sufficient for reaching the equilibrium. Sorption tests performed in bi-component equimolar solutions show that U(VI) can be strongly enriched on the sorbent at pH 4.9 while for Eu(III) metal binding is selective at pH 2.3 (but at the expense of a strong decrease in sorption capacity). The selective separation of these two metal ions (europium being representative of the behavior of REEs) is thus difficult but the sorbent can be considered a good support for the pre-separation of these metal ions. Metal ions can be readily desorbed using 0.5 M HCl solutions and the sorbent can easily be recycled: sorption and desorption performances are hardly altered after 5 successive cycles of sorption/desorption. The efficient recovery of uranyl from multi-component solutions produced by the alkaline leaching of low-grade sedimentary ores confirms the potential of this material for valorization of strategic metals.

This material seems to be very promising for metal recovery and separation from complex solutions; further tests will focus on the treatment of real-like effluents and mining leachates. A preliminary test carried out on the leachate of sedimentary uranium-containing ore confirmed this analysis. Another promising concept would consist of using chitosan beads functionalized with amidoxime groups for chromatographic-like columns in order to improve metal separation playing with both sorption and desorption steps.

Acknowledgement

Authors acknowledge the financial support from French Government through the post-doc fellowship attributed to Mohammed F. Hamza by the French Embassy in Cairo (Institut Français d'Egypte). Authors are also acknowledging the technical contribution of Thierry Vincent and André Brum (IMT Mines Ales, C2MA).

Appendix A. Supplementary data

Supplementary data associated with this article can be found, in the online version, at http://dx.doi.org/10.1016/j.cej.2018.03.029.

References

[1] A.G. Chmielewski, D. Wawszczak, M. Brykala, Possibility of uranium and rare metal recovery in the Polish copper mining industry, Hydrometallurgy 159 (2016) 12–18.
[2] M. Hadadian, M.H. Mallah, M.A. Moosavian, J. Safdari, M. Davoudi, Separation of uranium (VI) using dispersive liquid-liquid extraction from leach liquor, Prog. Nucl. Energy 90 (2016) 212–218.
[3] C. Tunsu, J.B. Lapp, C. Ekberg, T. Retegan, Selective separation of yttrium and europium using Cyanex 572 for applications in fluorescent lamp waste processing, Hydrometallurgy 166 (2016) 98–106.
[4] Z.W. Zhu, Y. Pranolo, C.Y. Cheng, Uranium recovery from strong acidic solutions by solvent extraction with Cyanex 923 and a modifier, Miner. Eng. 89 (2016) 77–83.
[5] S. Zhong, L. Bai, D. Zhao, L. Wang, Y. Li, L. Ding, Europium (III) coordination polymers micro/nanostructures: a ligand structure effect, Mater. Lett. 96 (2013) 125–127.
[6] A.N. Zagorodnyaya, Z.S. Abisheva, A.S. Sharipova, S.E. Sadykanova, Y.G. Bochevskaya, O.V. Atanova, Sorption of rhenium and uranium by strong base anion exchange resin from solutions with different anion compositions, Hydrometallurgy 131 (2013) 127–132.
[7] M.F. Attallah, E.H. Borai, S.A. Shady, Kinetic investigation for sorption of europium and samarium from aqueous solution using resorcinol-formaldehyde polymeric resin, J. Radioanal. Nucl. Chem. 299 (2014) 1927–1933.
[8] S.A. Ansari, P.K. Mohapatra, M. Iqbal, J. Huskens, W. Verboom, Sorption of americium(III) and europium(III) from nitric acid solutions by a novel diglycolamide-grafted silica-based resins: Part 2. Sorption isotherms, column and radiolytic stability studies, Radiochim. Acta 102 (2014) 903–910.
[9] Y. Wei, J. Qian, L. Huang, D. Hua, Bifunctional polymeric microspheres for efficient uranium sorption from aqueous solution: synergistic interaction of positive charge and amidoxime group, RSC Adv. 5 (2015) 64286–64292.
[10] M. Solgy, M. Taghizadeh, D. Ghoddocynejad, Adsorption of uranium(VI) from sulphate solutions using Amberlite IRA-402 resin: equilibrium, kinetics and thermodynamics study, Ann. Nucl. Energy 75 (2015) 132–138.
[11] K.K. Singh, S.K. Pathak, M. Kumar, A.K. Mahtele, S.C. Tripathi, P.N. Bajaj, Study of uranium sorption using D2EHPA-impregnated polymeric beads, J. Appl. Polym. Sci. 130 (2013) 3355–3364.
[12] M.G. Mahfouz, H.M. Killa, M.E. Sheta, A.H. Moustafa, A.A. Tolba, Synthesis, characterization, and application of polystyrene adsorbents containing tri-n-butylphosphate for solid-phase extraction of uranium (VI) from aqueous nitrate solutions, J. Radioanal. Nucl. Chem. 301 (2014) 739–749.
[13] A.A. Naser, G.E.S. El-Deen, A.A. Bhran, S.S. Metwally, A.M. El-Kamash,

Elaboration of impregnated composite for sorption of europium and neodymium ions from aqueous solutions, J. Ind. Eng. Chem. 32 (2015) 264–272.
[14] H. Catalette, J. Dumonceau, P. Ollar, Sorption of cesium, barium and europium on magnetite, J. Contam. Hydrol. 35 (1998) 151–159.
[15] C. Hurel, N. Marmier, Sorption of europium on a MX-80 bentonite sample: experimental and modelling results, J. Radioanal. Nucl. Chem. 284 (2010) 225–230.
[16] N.M. Kozhevnikova, Studying the sorption properties of a clinoptilolite-containing tuff with respect to europium(III) ions, Russ. J. Phys. Chem. A 88 (2014) 393–396.
[17] M.M. Hamed, M. Holiel, I.M. Ahmed, Sorption behavior of cesium, cobalt and europium radionuclides onto hydroxyl magnesium silicate, Radiochim. Acta 104 (2016) 873–890.
[18] P.K. Verma, P.K. Mohapatra, Effect of different complexing ligands on europium uptake from aqueous phase by kaolinite: batch sorption and fluorescence studies, RSC Adv. 6 (2016) 84464–84471.
[19] W. Lin, M. Carboni, C.W. Abney, K.M.L. Taylor-Pashow, J.L. Vivero-Escoto, Uranium sorption with functionalized mesoporous carbon materials, Ind. Eng. Chem. Res. 52 (2013) 15187–15197.
[20] T. Parsons-Moss, J. Wang, S. Jones, E. May, D. Olive, Z. Dai, M. Zavarin, A.B. Kersting, D. Zhao, H. Nitsche, Sorption interactions of plutonium and europium with ordered mesoporous carbon, J. Mater. Chem. A 2 (2014) 11209–11221.
[21] Z. Abdeen, Z.F. Akl, Uranium(VI) adsorption from aqueous solutions using poly (vinyl alcohol)/carbon nanotube composites, RSC Adv. 5 (2015) 74220–74229.
[22] K. Vijayaraghavan, M. Sathishkumar, R. Balasubramanian, Biosorption of lanthanum, cerium, europium, and ytterbium by a brown marine alga, *Turbinaria conoides*, Ind. Eng. Chem. Res. 49 (2010) 4405–4411.
[23] K. Vijayaraghavan, R. Balasubramanian, Single and binary biosorption of cerium and europium onto crab shell particles, Chem. Eng. J. 163 (2010) 337–343.
[24] V.A. Anagnostopoulos, B.D. Symeopoulos, Sorption of europium by malt spent rootlets, a low cost biosorbent: effect of pH, kinetics and equilibrium studies, J. Radioanal. Nucl. Chem. 295 (2013) 7–13.
[25] I.A. Erkaya, M.Y. Arica, A. Akbulut, G. Bayramoglu, Biosorption of uranium(VI) by free and entrapped *Chlamydomonas reinhardtii*: kinetic, equilibrium and thermodynamic studies, J. Radioanal. Nucl. Chem. 299 (2014) 1993–2003.
[26] E.I. Cadogan, C.-H. Lee, S.R. Popuri, H.-Y. Lin, Efficiencies of chitosan nanoparticles and crab shell particles in europium uptake from aqueous solutions through biosorption: synthesis and characterization, Int. Biodeterior. Biodegrad. 95 (2014) 232–240.
[27] E.I. Cadogan, C.-H. Lee, S.R. Popuri, Facile synthesis of chitosan derivatives and *Arthrobacter sp* biomass for the removal of europium(III) ions from aqueous solution through biosorption, Int. Biodeterior. Biodegrad. 102 (2015) 286–297.
[28] A.M. Atta, A.A.H. Abdel-Rahman, I.E. El Aassy, F.Y. Ahmed, M.F. Hamza, Adsorption properties of uranium (VI) ions on reactive crosslinked acrylamidoxime and acrylic acid copolymer resins, J. Dispersion Sci. Technol. 32 (2011) 84–94.
[29] A.A.H. Abdel-Rahman, A.M. Atta, I.E. El Aassy, F.Y. Ahmed, M.F. Hamza, Studies on the uptake of uranium(VI) ions on polyacrylamidoxime resins synthesized by free radical polymerization with different crosslinking ratios and pore solvents, J. Dispersion Sci. Technol. 32 (2011) 224–234.
[30] S.H. Choi, M.S. Choi, Y.T. Park, K.P. Lee, H.D. Kang, Adsorption of uranium ions by resins with amidoxime and amidoxime/carboxyl group prepared by radiation-induced polymerization, Radiat. Phys. Chem. 67 (2003) 387–390.
[31] S.H. Choi, Y.C. Nho, Adsorption of UO_2^{2+} by polyethylene adsorbents with amidoxime, carboxyl, and amidoxime/carboxyl group, Radiat. Phys. Chem. 57 (2000) 187–193.
[32] J. Kim, C. Tsouris, Y. Oyola, C.J. Janke, R.T. Mayes, S. Dai, G. Gill, L.-J. Kuo, J. Wood, K.-Y. Choe, E. Schneider, H. Lindner, Uptake of uranium from seawater by amidoxime-based polymeric adsorbent: field experiments, modeling, and updated economic assessment, Ind. Eng. Chem. Res. 53 (2014) 6076–6083.
[33] A.Y. Zhang, T. Asakura, G. Uchiyama, The adsorption mechanism of uranium(VI) from seawater on a macroporous fibrous polymeric adsorbent containing amidoxime chelating functional group, React. Funct. Polym. 57 (2003) 67–76.
[34] H.B. Pang, L.J. Kuo, C.M. Wai, N. Miyamoto, R. Joshi, J.R. Wood, J.E. Strivens, C.J. Janke, Y. Oyola, S. Das, R.T. Mayes, G.A. Gill, Elution of uranium and transition metals from amidoxime-based polymer adsorbents for sequestering uranium from seawater, Ind. Eng. Chem. Res. 55 (2016) 4313–4320.
[35] Y. Oyola, S. Dai, High surface-area amidoxime-based polymer fibers co-grafted with various acid monomers yielding increased adsorption capacity for the extraction of uranium from seawater, Dalton Trans. 45 (2016) 8824–8834.
[36] S.D. Alexandratos, X.P. Zhu, M. Florent, R. Sellin, Polymer-supported bifunctional amidoximes for the sorption of uranium from seawater, Ind. Eng. Chem. Res. 55 (2016) 4208–4216.
[37] Z.H. Zeng, Y.Q. Wei, L. Shen, D.B. Hua, Cationically charged poly(amidoxime)-grafted polypropylene nonwoven fabric for potential uranium extraction from seawater, Ind. Eng. Chem. Res. 54 (2015) 8699–8705.
[38] T.S. Anirudhan, M. Ramachandran, Synthesis and characterization of amidoximated polyacrylonitrile/organobentonite composite for Cu(II), Zn(II), and Cd(II) adsorption from aqueous solutions and industry wastewaters, Ind. Eng. Chem. Res. 47 (2008) 6175–6184.
[39] S.P. Mun, C.S. Ku, J.P. Kim, Adsorption of metal and uranyl ions onto amidoximated Pinus densiflora bark, Wood Sci. Technol. 44 (2010) 283–299.
[40] M.R. Lutfor, M.Y. Mashitah, Synthesis of poly(hydroxamic acid)-poly(amidoxime) chelating ligands for removal of metals from industrial wastewater, Eur. J. Chem. 8 (2011) 1038–1043.
[41] H.H. Abdel-Razik, E.R. Kenawy, Synthesis, characterization, and amidoximation of diaminomaleodinitrile-functionalized polyethylene terephthalate grafts for collecting heavy metals from wastewater, J. Appl. Polym. Sci. 125 (2012) 1136–1145.
[42] S.S. Metwally, R.R. Ayoub, H.F. Aly, Amidoximation of cyano group for chelating ion exchange of some heavy metal ions from wastewater, Sep. Sci. Technol. 48 (2013) 1829–1839.
[43] M. Ajmal, S. Demirci, M. Siddiq, N. Aktas, N. Sahiner, Amidoximated poly(acrylonitrile) particles for environmental applications: removal of heavy metal ions, dyes, and herbicides from water with different sources, J. Appl. Polym. Sci. 133 (2016).
[44] B. Wang, F. Zhang, J.-N. Wang, X.-Y. Li, C.-J. Li, Amidoxime-modified polyacrylonitrile nanofibers and application to Cr (VI) ions adsorption, Acta Polym. Sin. 1105–1111 (2016).
[45] A.H.A.-R. Adel, E.E.A. Ibrahim, Y.A. Fadia, F.H. Mohammed, Studies on the uptake of rare earth elements on polyacrylamidoxime resins from natural concentrate leachate solutions, J. Dispersion Sci. Technol. 31 (2010) 1128–1135.
[46] F.A. Alakhras, K. Abu Dari, M.S. Mubarak, Synthesis and chelating properties of some poly(amidoxime-hydroxamic acid) resins toward some trivalent lanthanide metal ions, J. Appl. Polym. Sci. 97 (2005) 691–696.
[47] B. Gao, X. Gao, Q. Lei, Studies on preparation of composite chelating material poly (amidoxime)/SiO_2 with grafting-type, J. Macromol. Sci., A 48 (2011) 119–127.
[48] M.F. Hamza, I.E. El Aassy, F.Y. Ahmed, A.A.H. Abdel-Rahman, A.M. Atta, Separation of uranium and rare earth elements with high purity from low-grade gibbsite-bearing shale ore by different chelating resins, J. Dispersion Sci. Technol. 33 (2012) 482–489.
[49] F. Li, Y. Dong, W. Kang, B. Cheng, X. Qu, G. Cui, Coordination kinetics of different metal ions with the amidoximated polyacrylonitrile nanofibrous membranes and catalytic behaviors of their complexes, Bull. Korean Chem. Soc. 37 (2016) 1934–1941.
[50] E. Guibal, Interactions of metal ions with chitosan-based sorbents: a review, Sep. Purif. Technol. 38 (2004) 43–74.
[51] F.-N. Allouche, E. Guibal, N. Mameri, Preparation of a new chitosan-based material and its application for mercury sorption, Colloids Surf., A 446 (2014) 224–232.
[52] C. Vincent, A. Hertz, T. Vincent, Y. Barre, E. Guibal, Immobilization of inorganic ion-exchanger into biopolymer foams – application to cesium sorption, Chem. Eng. J. 236 (2014) 202–211.
[53] M.D.S. Gama, F.M.T. Luna, J.Q. Albarelli, M.M. Beppu, R.S. Vieira, Adsorption of copper on glass beads coated with chitosan: stirred batch and fixed bed analysis, Can. J. Chem. Eng. 95 (2017) 1164–1170.
[54] Z.Y. Tan, H. Peng, H.F. Liu, L.L. Wang, J. Chen, X.H. Lu, Facile preparation of EDTA-functionalized chitosan magnetic adsorbent for removal of Pb(II), J. Appl. Polym. Sci. 132 (2015) art. 42384.
[55] A. Djelad, A. Morsli, M. Robitzer, A. Bengueddach, F. di Renzo, F. Quignard, Sorption of Cu(II) ions on chitosan-zeolite X composites: impact of gelling and drying conditions, Molecules 21 (2016).
[56] J. Xu, M. Chen, C. Zhang, Z. Yi, Adsorption of uranium(VI) from aqueous solution by diethylenetriamine-functionalized magnetic chitosan, J. Radioanal. Nucl. Chem. 298 (2013) 1375–1383.
[57] X. Zhang, C. Jiao, J. Wang, Q. Liu, R. Li, P. Yang, M. Zhang, Removal of uranium (VI) from aqueous solutions by magnetic Schiff base: kinetic and thermodynamic investigation, Chem. Eng. J. 198 (2012) 412–419.
[58] L. Fu, C. Shuang, F. Liu, A. Li, Y. Li, Y. Zhou, H. Song, Rapid removal of copper with magnetic poly-acrylic weak acid resin: quantitative role of bead radius on ion exchange, J. Hazard. Mater. 272 (2014) 102–111.
[59] K.Z. Elwakeel, A.A. Atia, Uptake of U(VI) from aqueous media by magnetic Schiff's base chitosan composite, J. Cleaner Prod. 70 (2014) 292–302.
[60] M.F. Hamza, A.A.H. Abdel-Rahman, S. Ramadan, H. Raslan, S. Wang, T. Vincent, E. Guibal, Functionalization of magnetic chitosan particles for the sorption of U (VI), Cu(II) and Zn(II)—Hydrazide derivative of glycine-grafted chitosan, Materials 10 (2017) 539–560.
[61] R. Massart, Preparation of aqueous magnetic liquids in alkaline and acidic media, IEEE Trans. Magn. 17 (1981) 1247–1249.
[62] A.M. Atta, A.A.H. Abdel-Rahman, M.F. Hamza, I.E. El Aassy, F.Y. Ahmed, Effect of crosslinker chemical structure and monomer compositions on adsorption of uranium (VI) ions based on reactive crosslinked acrylamidoxime acrylic acid resins, J. Dispersion Sci. Technol. 33 (2012) 490–496.
[63] M.V. Lopez-Ramon, F. Stoeckli, C. Moreno-Castilla, F. Carrasco-Marin, On the characterization of acidic and basic surface sites on carbons by various techniques, Carbon 37 (1999) 1215–1221.
[64] S. Lagergren, About the theory of so-called adsorption of soluble substances, Kungliga Svenska Vetenskapsakademiens 24 (1898) 1–39.
[65] Y.S. Ho, G. McKay, Pseudo-second order model for sorption processes, Proc. Biochem. 34 (1999) 451–465.
[66] C. Tien, Adsorption Calculations and Modeling, Butterworth-Heinemann, Newton, MA, 1994.
[67] I. Langmuir, The adsorption of gases on plane surfaces of glass, mica and platinum, J. Am. Chem. Soc. 40 (1918) 1361–1402.
[68] H.M.F. Freundlich, Uber die adsorption in lasungen, Z. Phys. Chem. 57 (1906) 385–470.
[69] C. Xu, J. Wang, T. Yang, X. Chen, X. Liu, X. Ding, Adsorption of uranium by amidoximated chitosan-grafted polyacrylonitrile, using response surface methodology, Carbohydr. Polym. 121 (2015) 79–85.
[70] A.K. Galwey, M.E. Brown, Thermal Decomposition of Ionic Solids – Chemical Properties and Reactivities of Ionic Crystalline Phases, 1st ed., Elsevier, Amsterdam, The Netherlands, 1999.
[71] G.Z. Kyzas, P.I. Siafaka, E.G. Pavlidou, K.J. Chrissafis, D.N. Bikiaris, Synthesis and adsorption application of succinyl-grafted chitosan for the simultaneous removal

of zinc and cationic dye from binary hazardous mixtures, Chem. Eng. J. 259 (2015) 438–448.
[72] Z. Zhang, Z. Dong, Y. Dai, S. Xiao, X. Cao, Y. Liu, W. Guo, M. Luo, Z. Le, Amidoxime-functionalized hydrothermal carbon materials for uranium removal from aqueous solution, RSC Adv. 6 (2016) 102462–102471.
[73] W.P. Li, X.Y. Han, X.Y. Wang, Y.Q. Wang, W.X. Wang, H. Xu, T.S. Tan, W.S. Wu, H.X. Zhang, Recovery of uranyl from aqueous solutions using amidoximated polyacrylonitrile/exfoliated Na-montmorillonite composite, Chem. Eng. J. 279 (2015) 735–746.
[74] G. Bayramoglu, A. Akbulut, M.Y. Arica, Study of polyethyleneimine- and amidoxime-functionalized hybrid biomass of *Spirulina (Arthrospira) platensis* for adsorption of uranium (VI) ion, Environ. Sci. Pollut. Res. 22 (2015) 17998–18010.
[75] G. Bayramoglu, M.Y. Arica, MCM-41 silica particles grafted with polyacrylonitrile: Modification in to amidoxime and carboxyl groups for enhanced uranium removal from aqueous medium, Microporous Mesoporous Mater. 226 (2016) 117–124.
[76] L. Hu, X.W. Yan, C.G. Yao, S.Y. Deng, X.M. Gao, X.J. Zhang, D. Shan, Preparation of amidoximated coaxial electrospun nanofibers for uranyl uptake and their electrochemical properties, Sep. Purif. Technol. 171 (2016) 44–51.
[77] X. Yin, J. Bai, W. Tian, S. Li, J. Wang, X. Wu, Y. Wang, F. Fan, Q. Huang, Z. Qin, Uranium sorption from saline lake brine by amidoximated silica, J. Radioanal. Nucl. Chem. 313 (2017) 113–121.
[78] S. Hokkanen, A. Bhatnagar, M. Sillanpaa, A review on modification methods to cellulose-based adsorbents to improve adsorption capacity, Water Res. 91 (2016) 156–173.
[79] J.B. Yang, B. Volesky, Biosorption of uranium on Sargassum biomass, Water Res. 33 (1999) 3357–3363.
[80] S. Liu, Y. Yang, T. Liu, W. Wu, Recovery of uranium(VI) from aqueous solution by 2-picolylamine functionalized polystyrene-co-maleic anhydride) resin, J. Colloid Interface Sci. 497 (2017) 385–392.
[81] G. Venkatesan, S. Pari, Growth of glycine ethyl ester hydrochloride and its characterizations, Phys. B 501 (2016) 26–33.
[82] X.J. Hu, J.S. Wang, Y.G. Liu, X. Li, G.M. Zeng, Z.L. Bao, X.X. Zeng, A.W. Chen, F. Long, Adsorption of chromium (VI) by ethylenediamine-modified cross-linked magnetic chitosan resin: Isotherms, kinetics and thermodynamics, J. Hazard. Mater. 185 (2011) 306–314.
[83] N. Mohammadi, A. Ganesan, C.T. Chantler, F. Wang, Differentiation of ferrocene D-5d and D-5h conformers using IR spectroscopy, J. Organomet. Chem. 713 (2012) 51–59.
[84] T.S. Xavier, P.T.M. Kenny, D. Manimaran, I.H. Joe, FT-IR and Raman spectroscopic and DFT studies of anti-cancer active molecule N-{(meta-ferrocenyl) Benzoyl} – L-alanine – glycine ethyl ester, Spectrochim. Acta, Part A 145 (2015) 523–530.
[85] J. Coates, Interpretation of infrared spectra, a practical approach, in: R.A. Meyers (Ed.), Encyclopedia of Analytical Chemistry, John Wiley & Sons Ltd, Chichester, U.K., 2000, pp. 10815–10837.
[86] G.H. Wang, J.S. Liu, X.G. Wang, Z.Y. Xie, N.S. Deng, Adsorption of uranium (VI) from aqueous solution onto cross-linked chitosan, J. Hazard. Mater. 168 (2009) 1053–1058.
[87] X. Xue, J. Wang, L. Mei, Z. Wang, K. Qi, B. Yang, Recognition and enrichment specificity of Fe_3O_4 magnetic nanoparticles surface modified by chitosan and *Staphylococcus aureus* enterotoxins A antiserum, Colloids Surf., B 103 (2013) 107–113.
[88] M. Namdeo, S.K. Bajpai, Chitosan-magnetite nanocomposites (CMNs) as magnetic carrier particles for removal of Fe(III) from aqueous solutions, Colloids Surf., A 320 (2008) 161–168.
[89] K. Oshita, T. Takayanagi, M. Oshima, S. Motomizu, Adsorption behavior of cationic and anionic species on chitosan resins possessing amino acid moieties, Anal. Sci. 23 (2007) 1431–1434.
[90] P.N. Pathak, G.R. Choppin, Sorption studies of europium(III) on hydrous silica, J. Radioanal. Nucl. Chem. 270 (2006) 277–283.
[91] V. Diniz, B. Volesky, Biosorption of La, Eu and Yb using *Sargassum* biomass, Water Res. 39 (2005) 239–247.
[92] S. Markai, Y. Andres, G. Montavon, B. Grambow, Study of the interaction between europium (III) and Bacillus subtilis: fixation sites, biosorption modeling and reversibility, J. Colloid Interface Sci. 262 (2003) 351–361.
[93] P. Sharma, G. Singh, R. Tomar, Synthesis and characterization of an analogue of heulandite: Sorption applications for thorium(IV), europium(III), samarium(II) and iron(III) recovery from aqueous waste, J. Colloid Interface Sci. 332 (2009) 298–308.
[94] R. Kautenburger, H.P. Beck, Influence of geochemical parameters on the sorption and desorption behaviour of europium and gadolinium onto kaolinite, J. Environ. Monit. 12 (2010) 1295–1301.
[95] B. El-Gammal, S.S. Metwally, H.F. Aly, S.A. Abo-El-Enein, Verification of double-shell model for sorption of cesium, cobalt, and europium ions on poly-acrylonitrile-based Ce(IV) phosphate from aqueous solutions, Desalin. Water Treat 46 (2012) 124–138.
[96] A.S. Suneesh, K.V. Syamala, K.A. Venkatesan, M.P. Antony, P.R.V. Rao, Diglycolamic acid modified silica gel for the separation of hazardous trivalent metal ions from aqueous solution, J. Colloid Interface Sci. 438 (2015) 55–60.
[97] A.S. Suneesh, K.V. Syamala, K.A. Venkatesan, M.P. Antony, P.R.V. Rao, Diglycolamic acid anchored on polyamine matrix for the mutual separation of Eu (III) and Am(III), Radiochim. Acta 104 (2016) 11–21.
[98] O. Abderrahim, N. Ferrah, M.A. Didi, D. Villemin, A new sorbent for europium nitrate extraction: phosphonic acid grafted on polystyrene resin, J. Radioanal. Nucl. Chem. 290 (2011) 267–275.
[99] C.L. Chen, X.K. Wang, M. Nagatsu, Europium adsorption on multiwall carbon nanotube/iron oxide magnetic composite in the presence of polyacrylic acid, Environ. Sci. Technol. 43 (2009) 2362–2367.
[100] S.A. Ansari, P.K. Mohapatra, Solid phase extraction of trivalent actinides and lanthanides using a novel CMPO-RTIL based chromatographic resin, Radiochim. Acta 101 (2013) 163–168.
[101] C. Xiong, Z. Zheng, Evaluation of D113 cation exchange resin for the removal of Eu (III) from aqueous solution, J. Rare Earths 28 (2010) 862–867.
[102] E. Guibal, I. Saucedo, M. Jansson Charrier, B. Delanghe, P. Lecloirec, Uranium and vanadium sorption by chitosan and derivatives, Water Sci. Technol. 30 (1994) 183–190.
[103] A.A. Atia, Studies on the interaction of mercury(II) and uranyl(II) with modified chitosan resins, Hydrometallurgy 80 (2005) 13–22.
[104] P. Metilda, K. Sanghamitra, J.M. Gladis, G.R.K. Naidu, T.P. Rao, Amberlite XAD-4 functionalized with succinic acid for the solid phase extractive preconcentration and separation of uranium(VI), Talanta 65 (2005) 192–200.
[105] M.A. Maheswari, M.S. Subramanian, AXAD-16-3,4-dihydroxy benzoyl methyl phosphonic acid: a selective preconcentrator for U and Th from acidic waste streams and environmental samples, React. Funct. Polym. 62 (2005) 105–114.
[106] A. Mellah, S. Chegrouche, M. Barkat, The removal of uranium(VI) from aqueous solutions onto activated carbon: Kinetic and thermodynamic investigations, J. Colloid Interface Sci. 296 (2006) 434–441.
[107] A.M. Donia, A.A. Atia, E.M.M. Moussa, A.M. El-Sherif, M.O.A. El-Magied, Removal of uranium(VI) from aqueous solutions using glycidyl methacrylate chelating resins, Hydrometallurgy 95 (2009) 183–189.
[108] L.C.B. Stopa, M. Yamaura, Uranium removal by chitosan impregnated with magnetite nanoparticles: adsorption and desorption, Int. J. Nucl. Energy Sci. Technol. 5 (2010) 283–289.
[109] M.K. Sureshkumar, D. Das, M.B. Mallia, P.C. Gupta, Adsorption of uranium from aqueous solution using chitosan-tripolyphosphate (CTPP) beads, J. Hazard. Mater. 184 (2010) 65–72.
[110] F. Semnani, Z. Asadi, M. Samadfam, H. Sepehrian, Uranium(VI) sorption behavior onto amberlite CG-400 anion exchange resin: Effects of pH, contact time, temperature and presence of phosphate, Ann. Nucl. Energy 48 (2012) 21–24.
[111] H. Wang, L. Ma, K. Cao, J. Geng, J. Liu, Q. Song, X. Yang, S. Li, Selective solid-phase extraction of uranium by salicylideneimine-functionalized hydrothermal carbon, J. Hazard. Mater. 229 (2012) 321–330.
[112] L. Zhou, C. Shang, Z. Liu, G. Huang, A.A. Adesina, Selective adsorption of uranium (VI) from aqueous solutions using the ion-imprinted magnetic chitosan resins, J. Colloid Interface Sci. 366 (2012) 165–172.
[113] W.H. Zou, L. Zhao, L. Zhu, Efficient uranium(VI) biosorption on grapefruit peel: kinetic study and thermodynamic parameters, J. Radioanal. Nucl. Chem. 292 (2012) 1303–1315.
[114] L. Ai, X. Luo, X. Lin, S. Zhang, Biosorption behaviors of uranium (VI) from aqueous solution by sunflower straw and insights of binding mechanism, J. Radioanal. Nucl. Chem. 298 (2013) 1823–1834.
[115] Q. Cao, Y. Liu, X. Kong, L. Zhou, H. Guo, Synthesis of phosphorus-modified poly (styrene-co-divinylbenzene) chelating resin and its adsorption properties of uranium(VI), J. Radioanal. Nucl. Chem. 298 (2013) 1137–1147.
[116] A.R. Keshtkar, M. Irani, M.A. Moosavian, Removal of uranium (VI) from aqueous solutions by adsorption using a novel electrospun PVA/TEOS/APTES hybrid nanofiber membrane: comparison with casting PVA/TEOS/APTES hybrid membrane, J. Radioanal. Nucl. Chem. 295 (2013) 563–571.
[117] N. Singh, K. Balasubramanian, An effective technique for removal and recovery of uranium(VI) from aqueous solution using cellulose-camphor soot nanofibers, RSC Adv. 4 (2014) 27691–27701.
[118] A.A. Galhoum, M.G. Mahfouz, N.A. Gomaa, S.S. Abdel-Rehem, A.A. Atia, T. Vincent, E. Guibal, Cysteine-functionalized chitosan magnetic nano-based particles for the recovery of uranium(VI): uptake kinetics and sorption isotherms, Sep. Sci. Technol. 50 (2015) 2776–2789.
[119] L. Li, N. Hu, D.X. Ding, X. Xin, Y.D. Wang, J.H. Xue, H. Zhang, Y. Tan, Adsorption and recovery of U(VI) from low concentration uranium solution by amidoxime modified Aspergillus niger, RSC Adv. 5 (2015) 65827–65839.
[120] H.-J. Liu, P.-F. Jing, X.-Y. Liu, K.-J. Du, Y.-K. Sun, Synthesis of beta-cyclodextrin functionalized silica gel and its application for adsorption of uranium(VI), J. Radioanal. Nucl. Chem. 310 (2016) 263–270.
[121] L. Sheng, L. Zhou, Z. Huang, Z. Liu, Q. Chen, G. Huang, A.A. Adesina, Facile synthesis of magnetic chitosan nano-particles functionalized with N/O-containing groups for efficient adsorption of U(VI) from aqueous solution, J. Radioanal. Nucl. Chem. 310 (2016) 1361–1371.
[122] X. Guo, Y. Feng, L. Ma, D. Gao, J. Jing, J. Yu, H. Sun, H. Gong, Y. Zhang, Phosphoryl functionalized mesoporous silica for uranium adsorption, Appl. Surf. Sci. 402 (2017) 53–60.